Quaternary Science Reviews
May 2018, Volume 187 Pages 1-30
https://doi.org/10.1016/j.quascirev.2018.03.018
https://archimer.ifremer.fr/doc/00495/60704/

Sediment failures within the Peach Slide (Barra Fan, NE Atlantic Ocean) and relation to the history of the British-Irish Ice Sheet

Owen Matthew J. [1, 4, *], Maslin Mark A. [1], Day Simon J. [2], Long David [3]

[1] UCL, Dept Geog, Gower St, London WC1E 6BT, England.
[2] UCL, Dept Earth Sci, Gower St, London WC1E 6BT, England.
[3] British Geol Survey, Murchison House,West Mains Rd, Edinburgh EH9 3LA, Midlothian, Scotland.
[4] Geol Survey Denmark & Greenland, C F Mollers Alle 8,Bldg 1110, DK-8000 Aarhus C, Denmark.

* Corresponding author : Matthew J. Owen, email address : mow@geus.dk

Abstract :

The Peach Slide is the largest known submarine mass movement on the British continental margin and is situated on the northern flank of the glacigenic Barra Fan. The Barra Fan is located on the northwest British continental margin and is subject to cyclonic ocean circulation, with distinct differences between the circulation during stadial and inter-stadial periods. The fan has experienced growth since continental uplift during the mid-Pliocene, with the majority of sediments deposited during the Pleistocene when the fan was a major depocentre for the British-Irish ice Sheet (BIIS). Surface and shallow sub-surface morphology of the fan has been mapped using newly digitised archival paper pinger and deep towed boomer sub-bottom profile records, side scan sonar and multibeam echosounder data. This process has allowed the interpretation and mapping of a number of different seismic facies, including: contourites, hemipelagites and debrites. Development of a radiocarbon based age model for the seismic stratigraphy constrains the occurrence of two periods of slope failure: the first at circa 21 ka cal BP, shortly after the BIIS's maximum advance during the deglaciation of the Hebrides Ice Stream; and the second between 12 and 11 ka cal BP at the termination of the Younger Dryas stadial. Comparison with other mass movement events, which have similar geological and oceanographic settings, suggests that important roles are played by contouritic and glacigenic sedimentation, deposited in inter-stadial and stadial periods respectively when different thermohaline regimes and sediment sources dominate. The effect of this switch in sedimentation is to rapidly deposit thick, low permeability, glacigenic layers above contourite and hemipelagite units. This process potentially produced excess pore pressure in the fan sediments and would have increased the likelihood of sediment failure via reduced shear strength and potential liquefaction.

Highlights

► A detailed and updated analysis of the Peach Slide. ► Two periods of sediment failure following the LGM: the first at ~21 ka cal BP and the second between 11 and 12 ka cal BP. ► Preferential accumulation of contourites within the Peach Slide Scar. ► Increased likelihood of failure via excess pore pressure produced by alternating glacigenic and contouritc sedimentation.

Keywords : Barra fan, Peach slide, Submarine mass movement, Quaternary, British-Irish Ice Sheet, Glaciation, North atlantic, Sedimentology-marine cores

1. Introduction

Submarine slope failures are a major component of the earth system with significant consequences with regard to tsunami generation (Bondevik et al., 2005; Bryn et al., 2005a), hazards to seabed infrastructure (Bea et al., 1983; Hsu et al., 2008) and possibly climatic change via the dissociation of methane-clathrate (Kennett, 2003). Understanding of the mechanisms governing the occurrence of these failures has improved significantly via detailed analysis of individual events (such as Storegga (Bryn et al., 2005a; Solheim et al., 2005)) as well as more extensive studies of multiple events (Canals et al., 2004; Chaytor et al., 2009; Lee, 2009; Masson et al., 2006; Owen et al., 2007; ten Brink et al., 2009; Urlaub et al., 2013). Some of these studies have shown a potential increased frequency of submarine mass movements on glaciated margins during and after deglaciation (Lee, 2009; Owen et al., 2007). However, it is widely acknowledged that there is still a need for detailed studies of submarine slope failures to extend the available database as well as to provide analogues for the potential impact of future climatic change.

Under a business as usual scenario, where it is assumed that future greenhouse gas emission trends follow those of the past, climate models forecast 8.3°C warming in the Arctic and 3.1°C warming in the Antarctic between 2081 and 2100 (IPCC, 2013, Chapter 12). Rapid ice melt is already observed in these regions, for example Greenland is losing over 200 gigatonnes of ice per year, a six-fold increase since the early 1990s, while Antarctica is losing about 150 gigatonnes of ice per year, a five-fold increase since the early 1990s (IPCC, 2013, Chapter 4). Meaning we may face deglaciation on a scale not observed since Termination 1A at circa 14 ka BP. As such, the deglaciation of a marine terminating ice sheet, during the last glacial period, with associated sedimentation, provides a suitable analogue for future submarine slope failures in polar regions.

To further these aims, of extending the database of well studied submarine mass movements and providing analogues for climatic change, this paper presents a detailed analysis of the Peach Slide. This is a large, and relatively unstudied, submarine mass movement complex situated within the Barra-Donegal Fan on the western continental margin of Britain and Ireland. On the basis of seabed and coastal glacial geomorphology it is inferred that during the Devensian the Barra-Donegal Fan was fed by marine terminating ice streams from the Hebrides, North Channel and northwest Ireland (Clark et al., 2012; Dove et al., 2015; Dunlop et al., 2010; Finlayson et al., 2014; Howe et al., 2012; Scourse et al., 2009; Small et al., 2017).

The Barra and Donegal Fans are frequently referred to as a single fan complex, taken as such the Barra-Donegal Fan Complex covers approximately 10,000 km^2 (location shown in Figure 1a). It has a thickness of ~650 m (Armishaw et al., 1998), it is the largest deposit of glacigenic sediment on the western British and Irish continental margin and the most southerly of the Trough Mouth Fans on the western European continental margin (Armishaw et al., 1998; Dahlgren et al., 2005). As this paper is concerned with sedimentation affecting the Barra sector of the complex the name Barra Fan is used throughout.

This paper builds on extensive previous work on the Peach Slide and includes a reanalysis of seismic and other geophysical data (see Owen et al., 2015) as well as new foraminiferal $\delta^{18}O$, particle size sedimentology and ^{14}C dates from a core in the Peach Slide headwall area (using methods presented by Owen et al., 2010; Owen, 2013). These new data are combined with key previous work in the area (Armishaw et al., 1998; Armishaw et al., 2000; Holmes et al., 1998; Knutz et al., 2002; Kroon et al., 2000) and recent studies on the growth, extent and deglaciation of the British-Irish Ice Sheet (BIIS) (Clark et al., 2012; Dove et al., 2015; Hughes et al., 2016; Small et al., 2017) to provide an updated geological model for sedimentation on the Barra Fan. This model is then used to investigate the timing and control of the two most recent slope failures within the Peach Slide complex.

2. Context and previous studies in the area

Figure 1a shows the Barra Fan location on the continental slope between the Hebrides Shelf and the Rockall Trough. To the north of the Barra Fan is the Hebrides slope and to the south are the Hebrides Terrace Seamount (HTS) and the Donegal Fan.

2.1. Geological setting

Following formation of northeast Atlantic, the northwest European margin and adjacent deep-water basins have undergone a structural evolution encompassing uplift and subsidence during different periods, which resulted in the strengthening of bottom current circulation in the Rockall Trough (Praeg et al., 2005; Stoker et al., 2010; Stoker et al., 2005a). The late-Pliocene to present uplift episode, is associated with the development of the Barra Fan (Dahlgren et al., 2005; Stoker et al., 2005b).

Contourite sedimentation dominates the successions of the northwest European margin from the intra-Miocene to intra-Pliocene unconformities, reflected in the characteristics of the RPb (Rockall and Porcupine Basins), FSN-2a (Faeroe-Shetland area) and Kai (North Sea Fan, Møre and Vøring Margins) formations (Bryn et al., 2005b; Stoker et al., 2005b).

Contour current formed features are visible on the Barra Fan's present seabed, with the Barra Fan drift a notable feature (Howe, 1996; Knutz et al., 2002). The region experiences a low level of seismic activity at the present time, though it is anticipated that this level increases during deglacial periods and for some millennia after (Bungum et al., 2010).

2.1.1. Glacial influence

Ice rafted debris (IRD) from the Rockall Plateau indicates that the margin has accumulated glacially derived sediment since ~2.6 Ma (Thierens et al., 2012). Although widespread glaciation of the Hebrides Shelf did not occur until the mid-Pleistocene. Evidence from BIIS sourced IRD supports a Hebrides shelf-grounded ice sheet during the Wolstonian glaciation, between 173 and 128 ka (Hibbert et al., 2010). The slope front glacigenic (post 0.44 Ma) deposits are termed the Upper Macleod sequence and consist of mid- to late-Pleistocene muds. These overlie the pre-glacial shallow marine sands of the Pliocene to early- to mid-Pleistocene Lower Macleod sequence (Stoker, 1995; Stoker et al., 1993). The uppermost unit on the Barra Fan is the Gwaelo Sequence, which overlies glacial debris flows (Stoker et al., 1993).

Indicated in Figure 1b, the Barra Fan consists primarily of sediments sourced from western Scotland and northwest Ireland (Howe et al., 2012; Knutz et al., 2001; Ó Cofaigh et al., 2012; Peters et al., 2008; Small et al., 2017). The Hebrides Shelf is incised by a number of deep trough features (North, Central and South Stanton Deeps and the Malin Deep shown in Figure 2a), believed to be eroded by ice-streams (Bradwell et al., 2008). Recent work (Dove et al., 2015; Howe et al., 2012; Small et al., 2017) provides evidence of ice-streams that flowed southwestwards through the Little Minch and the Sea of the Hebrides; and the presence on drumlins on the outer Malin shelf provides evidence of flow from northwest Ireland (Dunlop et al., 2010).

The BIIS is the primary source of the Barra Fan's sediment and glacial and deglacial periods represent key intervals with regards to fan sediment accumulation. Therefore, when considering slope stability on the fan it is necessary to consider the extent of ice-cover, as well as the timing, and nature of advance and retreat of the BIIS. Major growth of the ice-sheet occurred, after Heinrich event 4, from 38 ka cal BP (Peters et al., 2008; Scourse et al., 2009). Marine geophysical mapping on the Malin and Hebrides shelves, provides evidence indicating the period 29 - 26 ka cal BP as that of maximum ice extent, or the BIIS LGM (Clark et al., 2012; Hughes et al., 2016; Ó Cofaigh et al., 2012). Figure 1b, shows the shelf-edge northwestern extent of the BIIS as mapped by recent work (Bradwell et al., 2008; Clark et al., 2012). There is, however, uncertainty regarding ice

thickness on the Hebrides Shelf, with evidence suggesting that St Kilda (location shown in Figure 1b) was not overrun by the BIIS (Ballantyne et al., 2017; Hiemstra et al., 2015). This implies that it is unlikely to have reached the shelf edge in this west of Hebrides sector during the last LGM (Ballantyne et al., 2017).

Analysis of BIIS-sourced IRD clasts in core samples from the Rockall Trough and its environs provide timings that are broadly consistent with the geophysical mapping. BIIS IRD clast deposition is limited prior to Heinrich event 4, but increases between 30 and 28 ka and persists until 20 to 18 ka (Hall et al., 2011; Hibbert et al., 2010; Knutz et al., 2002; Knutz et al., 2007; Peck et al., 2007; Peters et al., 2008; Scourse et al., 2009), reflecting a probable shelf-edge advance and subsequent collapse. Evidence of a number of meltwater pulses within this period is presented by Knutz et al. (2007), Peck et al. (2007; 2008) and Hibbert et al. (2010) demonstrating the existence of localised, Heinrich-type events that would also be associated with rapid sediment deposition.

The age of the deglaciation, calculated from decline in BIIS IRD concentrations, is estimated at 18.4 - 17.2 ka cal BP (Peck et al., 2007) and 19 - 16 ka cal BP (Knutz et al., 2007). These ages correspond well with terrestrial data: evidence from cosmogenic ^{10}Be dating in Tiree show the Hebrides Ice Stream (HIS) to have deglaciated by 20.6 ± 1.2 ka cal BP (Small et al., 2017); whilst dating of moraines in northwestern Scotland provide an age of 17.9 to 15.5 ka cal BP for the first stable onshore position of the ice-sheet (Everest et al., 2006). Additional ^{36}Cl dating from Skye suggest that the Inner Hebrides component of the Barra Fan ice stream was deglaciated by 17.6 ± 1.3 ka cal BP (Small et al., 2016). These timings indicate a rapid retreat from the shelf-edge with rates in excess of 100 m a^{-1} (Clark et al., 2012). A stable onshore ice sheet does not preclude the possibility of an active marine-terminating ice-stream, as suggested to be possible, on the basis of IRD evidence, by Scourse et al. (2009).

On the basis of sea surface temperatures, reconstructed from planktonic foraminiferal assemblages, Kroon et al. (2000) place the warmer Bølling period slightly after 14.6 ka cal BP, the Younger Dryas cold period slightly after 13.5 ka cal BP and state that the Holocene was fully established by 10.9 ka cal BP (Kroon et al. (2000) ^{14}C dates converted using Fairbanks et al. (2005) radiocarbon calibration).

2.2. Oceanographic setting

As Figure 1 shows, the Rockall Trough is bounded by the continental shelf to the east, Rockall Bank in the west and the Wyville-Thomson Ridge in the north. Water depth increases from 1200 m in the north to 4500 m in the south. Water masses in the Rockall

Trough display an anti-clockwise cyclonic gyre, with eddies around banks and seamounts (Holliday et al., 2000).

The Rockall Trough is located within Atlantic Meridional Overturning system, with warm, saline water travelling northwards from the Caribbean and Gulf of Mexico, as the North Atlantic Current, and sinking in the Nordic Seas, before returning south as North Atlantic Deep Water (McManus et al., 2004). However, at a local level the picture is more complicated and operates at a number of different bathymetric levels. A summary of the contemporary circulation is presented in Figure 1c.

The majority of water masses that enter the Rockall Trough do so from the south. In the upper layers East North Atlantic Water is the major current, transported polewards with the Shelf Edge Current (SEC), contributing an average of 3.0 Sv of the mean upper water northerly flow of 3.7 Sv (Holliday et al., 2000; Øvrebø et al., 2006). The SEC typically displays flow speeds of 15 - 30 cm s^{-1} and is associated with the upper 400 - 500 m of the water column (Johnson et al., 2010; New and Smythe-Wright, 2001). Supporting this, Armishaw et al. (1998) document scour features, on the upper slopes of the Barra Fan, indicative of velocities of between 12 and 25 cm s^{-1}. The key intermediate water mass entering from the south is the cold and relatively fresh Labrador Sea Water (LSW), which occupies depths between approximately 1100 and 2200 m (Ullgren and White, 2010). Wyville-Thomson Overflow Water (WTOW) enters from the north of the Rockall Trough, is present at 600 - 1200 m depth and can be traced to at least 55°N (Johnson et al., 2010).

The dense Norwegian Sea Deep Water enters the Rockall Trough over the Wyville-Thomson Ridge (New and Smythe-Wright, 2001). As a consequence of mixing with surrounding water masses a salinity maximum is formed at 2300 - 2500 m water depth, this is associated with North East Atlantic Deep Water (NEADW) (Øvrebø et al., 2006). As with upper and intermediate water masses, deep water masses in the Rockall Trough display a cyclonic gyre with frequent eddies. High current speeds may be associated with these water masses, Dickson and McCave (1986) record velocities of up to 29 cm s^{-1} at 2500 m water depth in the southern Rockall Trough.

Driven by temperature and salinity gradients, it has been argued that freshening of the North Atlantic during deglaciations leads to a weakening of thermohaline circulation (Bond et al., 1993). In the North Atlantic, glacials are also associated with a reduction in deep convection and overflows from the Nordic Seas (Lynch-Stieglitz et al., 2007; McManus et al., 2004). Decreased deep ocean ventilation has also been observed at the onset of the Younger Dryas (Thornalley et al., 2010).

Analysis of the sortable silt fraction in the Rockall Trough by McCave et al. (1995) indicates vigorous intermediate water circulation during the last glacial, but more sluggish bottom water circulation. Further sedimentological evidence, supports the view of reduced bottom current flow in the Rockall Trough during glacials and stadials. Øvrebø et al. (2006), Knutz et al. (2002) and Armishaw et al. (2000) document a predominance of sandy contourite deposits (indicative of high current flow speeds) during the Holocene and of muddy contourites (indicative of low current flow speeds) during the glacial period.

2.3. Previous studies of the Barra Fan

The Barra Fan and Peach Slide have been the subject of a considerable body of previous work. Of most relevance to this study is work by Holmes et al. (1998), Armishaw et al. (1998; 2000) and Knutz et al. (2001; 2002). Holmes et al. (1998) present a key study that identifies Peach Debrites 1 - 4. The study maps the debrites and proposes approximate timing: early Pleistocene for Debrite 1 and post glacial for Debrite 4 (on the basis of iceberg scours truncated by the slide scar). Based primarily on regional airgun seismic lines, complimented with TOBI side scan sonar from the upper slope and the LOIS SES bathymetry of the slope between 56°N and 57°N, the authors map the extent and stratigraphic relation between Peach Debrites 1 – 4. Mapped extents as interpreted by Holmes et al. (1998) are shown in Figure 1b. This study also provides volume estimates: Debrite 1 at 835 km^3, Debrite 2 at 673 km^3, Debrite 3 at 199 km^3 and Debrite 4 at 135 km^3. There is some discussion of failure processes possible roles of increased pore pressure due to sediment loading and gas from Mesozoic growth faults beneath the fan. This work presents little detail regarding individual debrites.

An additional significant contribution to the understanding of the Barra Fan's sedimentology and morphology is presented in a body of work from Armishaw et al. (1998; 2000). The earliest of these two works presents an interpretation of fan surface and shallow sub-surface morphology based on pinger, TOBI side scan sonar and the LOIS SES bathymetry. The study interprets a number of echo facies including hemipelagites, interbedded hemipelagites and turbidites, debrites (and other deposits resulting from downslope transport) and contourites. This work is rigourous, however, it does not present any mapped facies distribution. A fact most likely due to the complexity of the facies geographical distribution and, as discussed in section 5.1, we disagree with some sub-bottom interpretations from the Peach Slide area. Armishaw et al. (2000) present an analysis of the Barra Fan and Peach Slide area sedimentary facies based on short core samples. This work is based on core transects (with individual samples often separated by

10s of kilometres). The key findings of this work are the presence of sandy and muddy contourites in the upper sediments, coupled with an absence of turbidites. As such, the study's main conclusions refer to the role of the alongslope currents in influencing the Holocene Barra Fan.

Knutz et al. (2001; 2002), present work investigating the timing of glacimarine sedimentation on the Barra Fan and the development of the Barra Fan Drift. A large part of this work is concerned with an analysis of the 30 m piston core MD95-2006, from which a ^{14}C age model is developed (Knutz et al., 2001). Additional work provided a seismo-stratigraphic age constraint of the Peach 3 Debrite, with emplacement calculated to be between 18 and 21 ka ^{14}C BP (Knutz et al., 2002).

The most recent of these studies was published in 2002 and prior to this study no significant work concerning the Peach Slide has been published since. Though additional work has be conducted in the area, including additional dates within piston core MD95-2006 (Austin et al., 2012; Wilson and Austin, 2002) and work by Maslin et al. (2004) that further refined the debrite ages using a crude seismic-stratigraphy correlation.

As well as providing the first detailed synthesis of previous work on the Peach Slide, this study goes further than this earlier work and provides four important additional contributions towards the understanding of these events:

i. Detailed mapping of the shallow sub-surface sedimentary facies extents and stratigraphic relations for the first time.

ii. New analysis of sediment core 56/ -10 /239, which penetrates a mass movement deposit in the headwall area of Peach 4. From this we present new ^{14}C dates, $\delta^{18}O$ and particle size data that helps to constrain the timing of Peach 4.

iii. Updated age model for fan and facies, compiling the published dates from the region, assessing the ^{14}C marine reservoir effect through time, converting these dates to calendar years and assigning these to the newly mapped seismic facies. This process has allowed a refinement of the timing of Peach 3 and 4, as well as much greater confidence in the accuracy of these dates.

iv. The first detailed discussion of the relationship between timing of sediment failure and oceanographic and glacial processes in the Peach Slide. This discussion draws on the recent body of work investigating the western sector of the last BIIS (as summarised section 2.1 and discussed in section 5.2).

3. Material and methods

This paper presents an updated interpretation of the surface and shallow sub-surface of the Barra Fan based on a combination of new data and a reanalysis of existing data sources. These are outlined below and an overview of the data sources used is presented in Figure 3.

3.1. Geophysical data

No new geophysical data were acquired for this study. Instead, a reanalysis of archival data has been performed taking advantage of more modern computer software and analysis techniques. Full details the workflow involved in this reanalysis are presented in Owen et al. (2015).

3.1.1. Bathymetry data

The primary bathymetric data source used by this thesis is the LOIS SES 3” bathymetric grid (BODC, 1999). The original dataset is a grid of tide corrected bathymetric depths spaced at 3” longitude by 3” latitude between 56° N and 57° N; and 9° 25’ W and 8° 55’ W. The data were collected between 02/03/1995 and 22/03/1995 (BODC, 1999). BODC ASCII data were converted into ESRI ASCII format and converted to raster data within ArcGIS. The LOIS SES 3” geographical grid corresponds to a grid resolution of 92 m north to south and 51 m east to west between 56° N and 57° N in UTM grid coordinates.

Detailed analysis of bathymetry (including gradients) within the study area is based solely on the LOIS SES dataset. In order to aid regional interpretation the LOIS SES data have been extended with bathymetry sourced from EMODnet (EMODnet, 2017).

3.1.2. Side scan sonar data

TOBI side scan sonar data from survey tranches 19-22 were acquired from the AFEN CD-ROM (AFEN, 1998). The TOBI survey was performed on the R.V. Colonel Templer between 12/06/1998 and 14/06/1998 (AFEN, 1998; Masson and Jacobs, 1998). Digital data in PDF format, gridded at 6 m resolution, were converted to TIFF files and then Geo-referenced in ArcGIS using the charted positional annotation as reference points.

3.1.3. Reanalysis of seismic data

Archival 3.5 kHz pinger sub-bottom profiler and deep-towed boomer paper records were acquired from the BGS (British Geological Survey) and NOC (National Oceanography Centre), scanned and converted to SEGY format (see Owen et al., 2015 for detailed description of method and assoicated uncertainties). The records totaled approximately

1600 km and were acquired between 1985 and 1998. Earlier data was acquired from the RRS Charles Darwin, during the first uses of GPS and the 1998 data was acquired from the R.V. Colonel Templer using DGPS positioning.

Once converted to SEGY the records were interpreted digitally using CODA Seismic+.

3.2. Sediment core data

3.2.1. Core selection

Prior to core selection and sub-sampling, logs of sediment cores were examined, alongside paper pinger records in the BGS Edinburgh laboratory during September 2006. Visual inspection determined that gravity core 56/-10/239 was most likely to achieve the study objectives, as it appeared to contain slumped material towards the core base and was located within the Peach Slide headwall area (see Figure 3). The core was acquired at 56° 46.93' N, 9° 10.19' W in 1030 m water during 1996.

Initial sub-sampling was performed at 2 cm intervals for the uppermost 2 m, with continuous 2 cm samples between 0.92 m - 0.98 m, 1.92 m - 1.98 m and 2.07 m - 2.13 m. Further sub-samples at 1 cm intervals, were obtained for the lowermost 0.5 m of the core.

3.2.2. Analytical methods

Particle size and bulk sediment x-ray fluorescence (XRF) analyses were undertaken at the UCL Geography department laboratory, $\delta^{18}O$ (and $\delta^{13}C$, not discussed here) analyses were performed at the UCL Bloomsbury Environmental Isotope Facility and AMS ^{14}C dating by the NERC Radiocarbon facility at East Kilbride.

3.2.2.1. Particle size analysis

Particle size analysis was performed without prior removal of carbonate content by acid leaching. This is consistent with the methodology of Howe (1996) and Armishaw (1999). Sediments are anticipated to be carbonate poor and there is potential for detrital limestone from Donegal within analysed sediments (Evans et al., 1983), which acid leaching would remove from the analysis potentially skewing the results.

Freeze-dried sub-samples were weighed and then wet-sieved through apertures of 1000, 500, 250, 125 and 63 µm before analysis of <63 µm diameter fraction by SediGraph 5120. Sediments from the wet sieved >250 µm fraction were subsequently dry sieved up to the maximum particle diameter.

Sub 63 µm fractions were covered and allowed to settle, before being split to 1 g - 2 g fractions in order to create a solution concentration of <3 % for SediGraph analysis

(Coakley and Syvitski, 1991). Particle density was assumed to be that of silica (the dominant element), at 2.32 g cm^{-3}. The GRADISTAT program (Blott and Pye, 2001) was used to calculate mean grain size, sorting, skewness and kurtosis.

3.2.2.2. *Foraminiferal stable isotope analysis*

$\delta^{18}O$ and $\delta^{13}C$ stable isotope analysis were measured on $CaCO_3$ tests from planktonic foraminiferal tests of both *Globigerina bulloides* and *Neogloboquadrina pachyderma (sinistral)*. *G. bulloides* is a surface dwelling sub-polar to temperate foraminifera, which calcifies in the uppermost 60 m of the water column (Schiebel et al., 1997); and *N. pachyderma (s.)* a sub-surface foraminifera common in polar and sub-polar water masses with calcification depths within the upper 200 m of the water column (Kohfeld et al., 1996).

Individuals were picked from the 250 µm to 500 µm fraction, however, when scarce *N. pachyderma (s.)* was also picked from the 250 µm to 125 µm fraction. Attempts were made to pick 30 individuals of each species per sample in order to achieve a $CaCO_3$ sample mass of 400 µg. Foraminiferal $CaCO_3$ samples were analysed for $\delta^{18}O$ and $\delta^{13}C$ using the UCL BEIF gas bench facility.

3.2.2.3. Foraminiferal ^{14}C dating

Funding was awarded for five foraminiferal $CaCO_3$ AMS ^{14}C dates under NERC allocation number 1441.1009. Insufficient $CaCO_3$ content meant that the samples below 2 m depth could not be submitted. The three submitted samples (16 – 18 cm, 156 – 158 cm, 196 – 198 cm) were analysed at the NERC radiocarbon facility at East Kilbride during April 2010. Following a query by NERC staff that sample SUERC-28180 contained 4 mg C as opposed to the recommended 5 mg C a new sample was submitted (194 – 198 cm) and analysed during July 2010.

3.2.3. Other core samples

In addition to BGS gravity core 56/-10/239 two other cores that have been discussed in published work are also incorporated into this study. These are BGS vibrocore 56/-10/36, analysed by Kroon et al. (1997; 2000); and piston core MD-95 2006 with published work presented by Kroon et al. (2000); Knutz et al. (2001; 2002); Wilson and Austin (2002); and Austin et al. (2012).

These additional cores are used to strengthen the age model and original ^{14}C dates are converted to calendar years using a more recent calibration curve (Bronk Ramsey, 2009) and updated marine reservoir corrections (see section 4.3 and Owen (2013)).

4. Results

4.1. Geophysical data

4.1.1. Bathymetry

As Figure 2a shows, in the study area the Hebrides Shelf margin is located between 9° and 9° 30’ W, with the Malin Shelf margin continuing to the south. To the east the Hebrides and Malin shelves have depths of less than 200 m, with the Stanton and Malin Deeps the areas of greatest depth. Between these areas, the Stanton Banks reach to within 50 m below mean sea level.

To the west of the continental margin is the Rockall Trough, which achieves depths of 2000 m below sea level within 50 km of the Hebrides Shelf. Situated around 56° 30’ N 10° 15’ W, the Hebrides Terrace seamount is a major bathymetric high located 50 km from the shelf break. As Figure 2 shows, this the summit of this feature has a diameter of some 20 km and rises from 1700 m to 1010 m below mean sea level on the eastern flank and from 2000 m on the western flank. Widely spaced contours between the Hebrides Terrace Seamount and the continental margin indicate the central location of the sedimentary fan, which engulfs the seamount, with the Barra Fan to the north and the Donegal Fan to the south.

Figure 2b shows more detailed imagery of the LOIS SES bathymetry between 56° N and 57° N. The main features apparent in the dataset are: gullies in the north; a landslide scar between these gullies and the smooth surfaced sediment fan to the south; and in the far south of the dataset: broad, deep gullies.

Regionally, the steepest gradients are located in the north of the LOIS SES bathymetry, where extensive areas display angles >10°. The gentlest slopes are located on the lower slope in the central fan area, where they are generally <2°. Locally the steepest slope angles are associated with the side walls of gullies and landslide scarps. In the northern gullied area angles reach 20°, whereas on the landslide scarp slopes they are commonly between 10° and 17°.

The LOIS SES bathymetry provides complete coverage for the large landslide scar within depths less than 1100 m below mean sea level. This covers the portion of the scar within the upper continental slope. As Figure 2b shows, the scar extends eastward, cutting back into the Hebrides Shelf creating an embayment within the continental margin. The scar area, at depths shallower that 1100 m below mean sea level is 210 km^2. In this upper region the maximum width of the evacuated area is 17.8 km. Relief is considerable, with

scarp heights of 73 m and 46 m in the north and south respectively. In the central headwall area, relief of 40 m is associated with mounded deposits. Slope angles associated with the scarp slopes are between 6° and 9° in the south and between 10° and 17° in the north. The southern scarps in particular are often associated with moats. There is no obvious join between the southern and northern scarps; an area of some 131 km^2 between the 900 m contour in the south (56° 38’ 52” N 9° 11’ 19” W) and the 650 m contour in the north (56° 42’ 58” N 9° 3’ 3” W) is obscured by downslope deposits from the upper slope. These deposits appear to originate from three upper scars, which reach the 200 m contour. The largest, and most pronounced, of these is the southernmost, which has an area of 36 km^2 and maximum scarp height of 80 m. This feature is 3.3 km wide and displays an evacuation zone of 3.5 km length and a depositional lobe of some 5 km length, with 20 m to 30 m elevation.

The continental margin in the far north and south of the study area is incised by numerous gullies, as shown in Figure 2b. These are discussed in more detail by Owen (2013).

4.1.2. Side scan sonar

AFEN Sidescan data are shown in Digital Supplement A.1. A number of artefacts are present in the data and these limit the degree of interpretation that is possible. A limited interpretation is presented in Digital Supplement A.2. The interpretation is combined with bathymetry and sub-surface results for the interpretation presented in section 5.1. Major features such as landslide scarps, debris deposits and large blocks are clearly visible within the sidescan data: extending the seabed interpretation beyond the limits of the LOIS SES dataset.

4.1.3. Description and characteristics of the seismic facies

Figures 4 to 8 show indicative examples of the seismic data with locations shown in Figures 2 and 3. Figure 4 shows a pinger line from the lower northern slopes of the fan. Here a transparent upper unit, 3.5 ms Two-Way-Travel-Time (TWTT) thick, drapes a unit characterised by parallel stratified reflectors unit some 12 ms TWTT thick. In turn, this unit drapes an uneven high amplitude reflector that displays a mounded morphology with some hyperbolic returns. This reflector masks the underlying material.

Figure 5 shows an example from the middle slopes of the fan at approximately 1400 m water depth. Here the upper unit’s reflectors are not noticeably different from the underlying seismic facies. However, a small lens-like feature is apparent at 4 ms TWTT below seabed in the north of the profile, it has a cross-sectional length of 200 m and a

height of ~2.5 ms TWTT. Below this a unit characterised by parallel reflectors continues and drapes the underlying surface. This unit is ~20 ms TWTT thick. Areas of apparent blanking are visible in the units lower sections. A more chaotic and semi-transparent unit, which displays a mounded upper morphology is apparent below the stratified unit. A lower reflector, which appears to represent a real geological feature is visible some 25 ms TWTT below the unit's upper surface. Towards the north of the profile a clear dipping reflector is visible within this chaotic unit. Further north still in the profile a number of vertically aligned areas of higher reflectivity are visible.

Figure 6 shows a pinger example from the continental slope above the southern slopes of the Barra Fan. An upper unit is largely transparent and drapes the underlying reflectors, though this upper unit displays a wavy upper surface. Below this unit is another that is characterised by a series of parallel reflectors of high and low amplitude of some 25 ms TWTT thickness. These reflectors appear folded and truncated on southern aspects. In the south of the profile, below these folded reflectors, is a chaotic semi-transparent unit.

Figure 7 shows a pinger data example from the northern margin of the Peach Slide area in water depths of 1250 m. Here a thin semi-transparent upper unit is occasionally visible, below which a ponded unit of up to 10 ms TWTT thickness is apparent. Below this unit declined reflectors are seen with noticeable offset, locations which are associated with significant surface gradient change.

Figure 8 displays a 10 km long profile running south to north, from the upper slopes of the Barra Fan into the Peach Slide headwall area in water depths of 500 m to 750 m. A steep and north dipping slope, of ~100 ms TWTT height is visible at fix 33. To the south of this feature are the slopes of the fan and to the north is the Peach Slide scar. The area south of the scarp is described first. Here a thin upper unit, of relatively high amplitude drapes a stratified unit some 15 ms TWTT thick. Areas of blanking are visible in this stratified unit. Below this a semi-transparent chaotic unit that displays a mounded upper morphology is visible, where it reaches maximum thickness underlying reflectors are obscured. Towards this unit's margins, where it is less thick a further parallel stratified unit is visible, the reflectors of which are truncated at the prominent scarp. South of the scarp units show more deformation. An upper unit shows indications of surface erosion and drift formation (see fix 36 in Figure 4) where it thickens to 14 ms TWTT. Below this unit is a stratified unit, up to 25 ms TWTT thick, which displays internal offsets along with areas of high amplitude and blanking. Below this unit a chaotic, semi-transparent unit is occasionally visible. Where this unit is absent deeper, folded reflectors are apparent.

On the basis of the observed character six seismic facies (FI to FVI) are interpreted, of which Facies IV is divided into three sub-facies (IVa to IVc) and Facies VI into two (VIa and VIb). These are outlined in Figure 9 and Table 1. Not shown in data examples in this paper are facies IVb, a chaotic, semi-transparent unit displaying a flat or convex down upper morphology; and facies VIb, seismic blanking associated with a fault. Inferred origin of the interpreted facies are discussed in section 5.1.

As this paper is concerned with the shallow subsurface morphology of the Barra Fan a uniform velocity of 1525 m s^{-1} is assumed. This is based on the measured velocity of units in core sample MD95-2006 as presented by Knutz et al. (2002).

4.2. Gravity core 56/-10/239

Figure 10 displays a summary of the sedimentology and geochemical results from core sample 56/-10/239.

4.2.1. Sedimentology

On the basis of sand, silt and clay composition shown in Figure 10b, CS 56/-10/239 can be broadly divided into six units.

i. From base of core, at 2.50 m, to 2.03 m a unit of dense and deformed clay intraclasts with sandy matrices. It consists of mud to sandy gravelly mud that contains up to 65.3% clay, though with variable sand values that reach 26.2%. Mean grain size oscillates between 8.0 ϕ and 6.5 ϕ, mirrored in the sorting (σ_I) with more sorted sediments associated with finer grain size.

ii. From 2.03 m to 2.00 m a pronounced layer of slightly gravelly muddy sand, with shell fragments, that erodes into the unit below. The sub-sample at 2.00 m - 2.01 m contains the maximum sand content in the core of 82.2%. Mean grain size increases to 2.8 ϕ and the unit is poorly sorted.

iii. Between 2.00 m and 1.58 m a unit of alternating sandy clay and silty clay, moving up core the unit displays a decline in the proportion of sand and an increase in silt; which is the dominant particle fraction between 1.68 and 1.82 m. Mean grain size increases from 7.0 ϕ to 5.5 ϕ, there is a slight decline in sorting from 2.0 σ_I to 2.5 σ_I.

iv. From 1.58 m to 0.97 m two upwards fining sequences, from slightly gravelly sandy mud to mud. An initial increase in sand at 1.53 m is followed by increased proportions of silt and clay, which reaches 48.8% at between 1.34 m and 1.32 m. A further increase in sand occurs at 1.25 m, followed by an upwards fining sequence to

0.97 m. There is a stepped fining of mean grain size to 7.6 ϕ at 1.13 m after which it is relatively constant. Sediment sorting is relatively constant around 2.7 σ_I.

v. Between 0.97 m - 0.16 m there is a sandy mud sequence dominated by clays and silts, though with occasional elevated sand values (for instance 23.9% at 0.49 m). The unit has a distinct upper boundary and more poorly defined lower boundary. Mean grain size is relatively consistent at 7.2 ϕ and sorting is also consistently around 2.7 σ_I.

vi. From 0.16 m a unit of muddy sand is apparent, sand reaching a maximum value of 64.0% at the topmost sub-sample. Sediment mean grain size increases to 4 ϕ at top of core and sediments become less sorted.

4.2.2. Planktonic foraminiferal $\delta^{18}O$

Shown in Figure 10d, *N. pachyderma (s.)* displays heavier $\delta^{18}O$ values than *G. bulloides*, as is anticipated from the species' greater calcification depth (Kohfeld et al., 1996; Schiebel et al., 1997). For both species, the isotopically heaviest values are observed towards the base of core (4.36‰ VPDB for *N. pachyderma (s.)* and 3.39‰ VPDB for *G. bulloides*). Though below 2.00 m, *G. bulloides* is generally absent. *N. pachyderma (s.)* is absent between 1.84 m and 1.41 m. $\delta^{18}O$ values decrease upwards through the core. In the case of *N. pachyderma (s.)*, from ~4.0‰ to ~3.0‰ and from ~3.5‰ to ~1‰ in the case of *G. bulloides*. Though there is an apparent increase of 0.5‰ in both species' $\delta^{18}O$ between 1.38 m and 1.00 m. Minimum values are observed at 0.21 m, above which point $\delta^{18}O$ values become isotopically heavier.

4.2.3. Radiocarbon analysis of 56/-10/239

Results of AMS ^{14}C dating are shown on Figure 10, and summarised in Table 2. As shown by the youngest recorded date (10688 ± 44 years ^{14}C BP) occurring at 1.96 – 1.98 m depth and the oldest recorded date (12889 ± 43 years ^{14}C BP) occurring at 1.56 – 1.58 m there is a discontinuity within the core. This and the marine reservoir effect are discussed further in section 4.3.

4.3. Existing core samples and ^{14}C chronology

4.3.1. Marine reservoir effect

There is a large degree of uncertainty concerning temporal variation of the marine reservoir effect at the Barra Fan. Estimates of the magnitude of the effect are based on a variety of data types, including: comparison between marine AMS ^{14}C dates and terrestrial

carbon (Bondevik et al., 2006), corals (Cao et al., 2007), tephra (Austin et al., 1995; Austin et al., 2011), Greenland ice-cores (Björck et al., 2003; Hall et al., 2011) and modeled data (Franke et al., 2008).

In addition to these published data it is possible to estimate the marine reservoir effect in the Northeast Atlantic, during marine isotope stage 2, from the Fugloyarbanki tephra layer, dated at 26,690 cal BP in the NGRIP ice core by Davies et al. (2008). Austin et al. (2012) demonstrate that MD95-2006 samples this layer at 19.30 m. As the tephra layer in MD95-2006 is situated between two planktonic foraminiferal AMS ^{14}C dates one can interpolate linearly between these, assuming that there is a constant sedimentation rate and that the reservoir effect is unchanged during the sampled time period. This exercise has been performed and a reservoir correction of between 900 and 1000 years is required to calibrate the marine tephra layer to the NGRIP record (see Owen, 2013 for details).

Though this is approach is crude it does provide a value consistent with increased reservoir effect due to southerly migration of the polar front, reduced North Atlantic meridional overturning and with pre-bomb Arctic data (Bard et al., 1994; Hughen et al., 2004). The value is roughly half of that demonstrated in the Rosemary Bank - GISP2 comparison performed by Hall et al. (2011), this difference may be due to the more northerly location of Rosemary Bank. Due to the Barra Fan location the Fugloyarbanki derived correction is used. This study uses different corrections for distinct time periods that are outlined in Table 3, uncertainty regarding the reliability of these corrections increases with age.

4.3.2. Core chronology

Figure 11 shows summary logs of MD95-2006 and 56/-10/36 for comparison with the previously discussed details of 56/-10/239. Table 4 provides a summary of all the dating (^{14}C and tephra) used in this study alongside the reservoir correction and calculated calendar age. A 30 m piston core, MD95-2006 covers the late glacial and Holocene with 18 dated samples ranging from 33.88 ka ^{14}C BP to 2.80 ka ^{14}C BP (Austin et al., 2012; Knutz et al., 2001) and is located on the lower slopes of the Barra Fan. Vibrocore 56/-10/36 is 5 m long with six dated samples ranging from 13.02 ka ^{14}C BP to 10.04 ka ^{14}C BP (Kroon et al., 1997) and is situated in 1300 m of water on the mid-slopes of the Barra Fan.

Due to the location of 56/-10/36 within the area bounded by the prominent landslide scarp it would be expected that this core would provide a minimum age for the emplacement of Peach 4 (Owen et al., 2010). However, on analysing the data more closely it seems that

the core does not match the nearby seismic data, which indicates a hard seabed as opposed to the soft material sampled by the core. This could be due to the distance between the core position and seismic lines (200 m and 600 m) or navigational inaccuracies associated with Decca system, used in 1985 when the core was acquired, which could be up to 1 nautical mile: sufficient distance to position the core away from the interpreted mass movement deposits (Figure 11). It seems more likely that the core samples sediments that have undergone more limited movement, perhaps equivalent to the lateral spreading or more gradual down-slope creep. On this basis it seems that the core does not directly constrain the age of Peach 4.

Discussed in section 4.2, gravity core 56/-10/239 shows the presence of mass movement deposits, consisting of glacial age material (on the basis of full glacial foraminiferal $\delta^{18}O$ values) and visible deformation of clay intraclasts, below 2.0 m and deposited prior to 10.69 ka ^{14}C BP. The core stratigraphy is complicated, with an age reversal observed at 1.57 m within the core, demonstrating an additional mass movement and emplacement event.

4.3.3. Facies age constraint based on core and geophysical results

An age model for the study area has been constructed on the basis of ^{14}C dating of the three core samples discussed above and the observed seismic stratigraphy.

Interpretation of piston core MD95-2006, by Knutz et al. (2002) is extremely useful to this study and assists in producing a more accurate chronological framework. Comparison with the associated pinger and deep towed boomer data (Digital Supplement B) allows this interpretation (see Figure 11) to be linked with the seismic facies interpretation presented here.

Knutz et al.'s (2002) upper contourite unit and seismic unit I-A are, respectively, equivalent to seismic facies I and IIa interpreted here. The chronology established for this core (Austin et al., 2012; Knutz et al., 2001; Knutz et al., 2002; Wilson and Austin, 2002) may, therefore, be used to constrain the ages of seismic facies Ia and IIa interpreted in this study. Vibrocore 56/-10/36 also samples an upper contourite unit, in this case ~1 m thick. This is the equivalent of interpreted seismic facies I. Table 5 shows facies age constraint based on the calendar ages shown in Table 4 and the seismic data shown in Figures 4 to 8.

5. Discussion

Having obtained and interpreted seismic data and built an appropriate radiocarbon based age model it is possible to determine the origin of the different seismic facies. This provides some key insights into the processes operating on the Barra Fan and the relative influence of glacial-inter-glacial sedimentation regimes and relative sea level changes.

5.1. Origin, occurrence and age of seismic facies

As the internal structure and geometry of a sedimentary unit is often determined by a unit's depositional process we now consider the seismic facies and whether a sedimentary unit's reflective character may be indicative of a given sedimentology. The seismic interpretation presented here builds on previous work from the Barra Fan (Armishaw, 1999; Armishaw et al., 1998; Howe, 1996; Knutz et al., 2002) and the Nova Scotian margin (Tripsanas et al., 2008; Tripsanas et al., 2007). Examples of the interpreted facies are shown in Figure 9 and these are summarised in Table 1.

5.1.1. Facies I – contourite

5.1.1.1. Origin

Seismic facies I is interpreted where the base of the uppermost unit in the sedimentary column clearly drapes the underlying units and has a clear basal reflector that differentiates it from the units below. This prominent reflector indicates a change in seismic impedance and sedimentation process. As shown in Figures 4 and 9, this unit may overlie seismic facies II, which it is differentiated from by a lack of laminations.

The facies is generally <4 ms TWTT thick and not always present (see Figure 12 for isopach at 1 km resolution). At times the unit displays asymmetry, an eroded upper surface and may contain bedforms (Figures 6 and 8). This unit may display low (largely transparent) or high amplitudes. As such this study interprets seismic facies Ia and Ib, low and high amplitudes respectively.

Ground truthing of this unit is attempted via the published core sample records from the region. Armishaw et al. (2000) present 24 core logs from the Barra Fan and Peach Slide that document a thin (<0.5 m) uppermost sandy contourite unit, which overlies muddier sediments (contouritic, hemipelagic or glaciogenic). At the northern edge of the Barra Fan, Howe (1996) shows seven core logs that indicate the presence of a 0.1 - 0.4 m thick, poorly sorted, foraminiferal rich sand layer overlying muddier sediments (hemipelagic and hemiturbidite). Knutz et al. (2002) describe piston core MD95-2006, recovered from 2130

m water depth at the northwest margin of the Barra Fan; they describe a silty-muddy contourite unit, ~1.5 m thick, overlying a 4 m thick sequence of hemipelagic muds grading into muddy contourites.

The prominent reflector that defines the unit's base may indicate a period of increased current velocity, resulting in sediment winnowing and development of lag deposits. On the basis of reflective characteristics, unit geometry and the sediment core interpretations described above seismic FIa and FIb are interpreted as muddy and sandy contourites respectively.

In some locations the facies thickens; and in these instances consideration was given as to whether the facies could indicate debris flow deposition. Wavy reflectors, characteristic of some contourite deposits, are not generally visible within the unit, though in a muddy contourite the low internal reflection co-efficient results in a seismically transparent facies (Rebesco and Stow, 2001; Stow and Faugères, 2008). The interpreted unit also lacks characteristics associated with debris flow deposits (see Amy et al., 2005; Iverson et al., 2010). Asymmetry of FI deposits in Figure 4 is similar to that described by Dorn and Werner (1993) for deposits on the Faeroe-Iceland Ridge; and the thinning of the FI unit adjacent to the landslide scarp in Figure 8 and on the continental slope (Figure 7) bares marked similarity to erosional scour documented in the Sicily Channel by Marani et al. (1993). Additionally, shown in Figure 8, the interpreted FI facies, consisting of small scale drifts overlying a generally uniform drape, is strikingly different from the mounded debris flow facies (FIVa) below.

It is recognised that sedimentation processes operate in a spectrum and that, as recognised by Armishaw et al. (2000) and Knutz et al. (2002), the Barra Fan is subject to downslope and across slope transport mechanisms. As such it is highly probable that sediments within the slide scar originate from a number of sources and have been transported via a combination of processes.

5.1.1.2. Occurrence

Thicknesses of FI are shown in comparison to surface morphology in Figure 12. Facies I is largely absent from the southern slopes of the Barra Fan, where there is no clear distinction from the laterally correlated FIIa. Conversely, to the north of the Barra Fan FI is observed frequently and achieves significant thicknesses, particularly within the landslide scar. However, as demonstrated by Figure 12, there is variation with some areas having

deposits >9 m thick and other areas, such as in deeper than 1500 m in the slide scar, <2 m thick or absent.

5.1.1.3. Age constraint

Evidence from sediment cores suggest that enhanced contourite sedimentation is generally associated with the transition to interglacial conditions. Knutz et al. (2002) for example at a water depth of 2130 m identify a silty, muddy contourite in the upper 1.5 m of core sample MD95-2006 (Figure 11); the base of which is dated at 11.3 ka cal BP (Wilson and Austin, 2002). Closer to the shelf edge, at 1320 m water depth, Kroon et al. (2000) date the base of a thin contourite unit in core sample 56/-10/36 at 11.4 ka cal BP (Figure 11).

The evidence cited above indicates an age of approximately 11.4 ka cal BP for the onset of post-glacial contourite deposition on the Barra Fan and, hence, for the base of seismic facies I.

5.1.2. Facies II - hemipelagite

5.1.2.1. Origin

This facies is present in the upper sedimentary column, is of relatively low seismic amplitude and drapes underlying units with parallel reflectors (Figures 4 and 5). Where present, it is generally between 10 and 50 ms TWTT thick, though thickness is commonly ~25 ms TWTT (20 m at a seismic velocity of 1525 m s^{-1}). Displaying a draped morphology this unit is probably hemipelagic in origin. Generally underlying seismic FI, ground truthing of FII is rare due to the low number of core samples >2.5 m length, but piston core MD95-2006, presented by Knutz et al. (2002), penetrates a unit that is equivalent to FII (see Digital Supplement B and section 4.3.3). Knutz et al.'s (2002) Seismic unit IA is a stratified drape and consists of glacimarine clays merging upwards into contourites.

5.1.2.2. Occurrence

Facies IIa is interpreted over large areas within the study area. However, it is interpreted as absent on steep slopes and where debris and debris flows occur at or near the surface, such as within landslide scars in the south and centre of the study area. At times, interpreted depth is limited by seismic penetration.

5.1.2.3. Age constraint

Further north, on the Hebrides slope, Stoker et al. (1994) present a seismic stratigraphy interpreted with borehole 88/7.7A, where the upper 20 m of the sedimentary column is dominated by sedimentation during the Devensian. The seismic record shown by Stoker et al. (1994) is very similar to the pinger records from the Barra Fan. This suggests that seismic facies II may consist of sediments deposited during the last glacial transition and represents the Gwaelo sequence (Stoker et al., 1993). This is consistent with the chronology presented by Knutz et al. (2002).

This unit rests above material dated at 19.95 ka cal BP (based on converting Wilson and Austin, 2002 ^{14}C date to calendar years) and the lowermost ^{14}C date in this unit yields a calendar age of 18 ka cal BP. Using the argument that FIIa is equivalent to Knutz et al. (2002) seismic unit I-A and the Gwaelo sequence interpreted by Stoker et al. (1993), it can be dated as younger than 19.95 ka cal BP. Therefore, the unit consists of sediments deposited during the deglacial transition (including intervals of ice advance and retreat, as outlined in section 2.1) prior to deposition of contourite sediments during the Pre-Boreal and Holocene.

5.1.3. Facies III – turbidites or sandy contourites

A high amplitude seismic facies III is interpreted to consist of coarser sediments. An example from the upper sedimentary column is shown in Figure 9. On the Barra Fan coarser sediments are most likely deposited via sandy contourites or turbidites. It is extremely difficult to distinguish between these two types without ground truthing via sediment samples. This facies is not determined by stratigraphic position, therefore no age constraint is given.

5.1.4. Facies IV and V – mass movement related deposits and features

5.1.4.1. Origin

Seismic facies IV, which is divided into three sub-facies, consists of chaotic semi-transparent facies; of which examples are shown in Figures 4 to 9. Thickness of this facies varies from 1 - 2 ms TWTT to 50 ms TWTT or more (this facies often extends beyond the limit of the pinger record's penetration). Morphology of the facies varies from ponded with slightly convex down upper boundaries (see Figure 9) to mounded forms with convex upper boundaries (See Figures 4 to 8). From the basis of the seismic characteristics this unit is interpreted as being a debris flow deposit, or debrite.

No existing core samples penetrate this facies, therefore ground truthing is not possible. However, referral to the mass transport facies literature allows more precise interpretation. Numerous continental margin studies have demonstrated that chaotic, semi-transparent to transparent, seismic facies are indicative of debris flow deposits (Canals et al., 2004; Laberg et al., 2002b; Piper et al., 1999). From interpreting seismic characteristics of these facies in more detail it is possible to further refine the debris flow interpretation. For example, mass transport deposits on the Nova Scotian margin have been investigated in detail using seismic data and core samples (Jenner et al., 2007; Tripsanas et al., 2008; Tripsanas et al., 2007). Tripsanas et al. (2007) differentiate between low and high viscosity cohesive debris flows; the deposits of which they distinguish on the seismic record with low viscosity flows displaying flat to convex down upper surfaces and high viscosity flows exhibiting slightly convex up upper surfaces and hyperbolae.

Based on the seismic characteristics observed in the Barra Fan data, and insights from the seismic facies literature, this paper interprets three sub-classes of chaotic semi-transparent facies. Seismic facies IVa and IVb are interpreted as deposits from high viscosity cohesive debris flows and low viscosity cohesive debris flows respectively, they are differentiated on the basis of upper surface morphology (convex up to down) and presence of hyperbolae. A further facies, IVc, is interpreted to identify prominent internal reflectors within the debris flow units.

Seismic facies V displays high amplitude, irregular hyperbolic returns. The facies is observed on the seabed (Figure 9) as well as within the sedimentary column. Presence of this facies normally prevents any further seismic penetration. The presence of irregular hyperbolic reflectors in the seismic record is generally an indication of blocks within the sediment or rugged terrain (Damuth, 1978). These blocks may consist of individual boulders or rafted sediment blocks (Tripsanas et al., 2007). This paper interprets these irregular hyperbolic returns as hard debris.

5.1.4.2. Occurrence

Mass movement facies (FIVa, FIVb, FIVc and FV) are observed at varying depths within the stratigraphic column and in different geographical locations as shown in Figure 13. The mass movement facies observed on the seabed (Figure 13a) include debrites, blocky debris and slumped hemipelagic material. Debrites observed at the seabed on the Barra Fan appear to pond in bathymetric depressions and often display a convex down upper boundary, as such they are interpreted to have been deposited by low viscosity (FIVb) debris flows. The debrites located within the landslide scars in the south and central north

of the study display greater relief, more hyperbolae and are interpreted to have been deposited by high viscosity (FIVa) debris flows. A smaller area of debris and debris flow deposits is observed on the east flank of the Hebrides Terrace seamount. Mass movement facies underlying the surface contourite unit are shown in Figure 13b. These consist of debrites and blocky debris and are located in two main areas. First, in the centre and north of the study area, associated with the landslide area. Second, in the south of the study area, associated with and downslope from, the area of gullies and landslide scars. Those debris and debrite facies that underlie the hemipelagic unit are shown in Figure 13c. These features extend downslope from the upper slopes of the Barra Fan. They are absent from the upper slopes of the landslide area, but present on the lower slopes. Denser material will reduce pinger sub-surface penetration and interpretation of these deeper units, from pinger data, within the landslide area is not possible.

Shallow faults are interpreted throughout the study area, though obvious vertical displacement is not commonly imaged. In part this may be due to data resolution issues resulting from the significant water depth, however, it may also reflect the presence of tension fractures and lateral spreading. Intact blocks are also visible, some, such as those shown in Figure 7, have undergone limited downslope movement and may indicate extensional faulting following the removal of the toe of the slope. Other blocks appear to have been transported as rafts within a debris flow matrix and have potentially travelled tens of kilometres (see side scan sonar examples in Digital Supplement A).

Hyperbolic seismic returns, exposed on the seabed and buried within debris flow deposits, as well as large scale blocks visible in the side scan data suggest the presence of blocky debris.

5.1.4.3. Age constraint

The age of these facies may be determined based on their stratigraphic position relative to facies I and II. As shown in Figure 14, the mass movement facies interpreted here are associated with a number of different seismostratigraphic positions. The oldest of those visible occur prior to the deposition of FIIa, which drapes the mass movement deposits. Debris flow facies are rarely observed within the stratified FIIa unit, though areas of higher amplitude reflection may indicate some coarser grained turbidite deposition. Extensive debrites are observed immediately above FIIa, some of which are capped by FI. Other instances of mass movement facies are observed on the seabed (see Figure 13).

Caution must be used when bracketing the age of mass movement deposits via the adjacent hemipelagic or contouritic units. Hiatuses in the sedimentary column are possible and Knutz et al. (2002) note erosion of seabed sediments by bottom currents, though there is no evidence of this in the cores analysed in this study. The predominance of sandy contourite facies in recent sediments on the Barra Fan (Armishaw et al., 2000) and measured current velocities of 29 cm s^{-1} at 2500 m water depth within the Rockall Trough (Dickson and McCave, 1986) indicate the potential for erosion. Therefore, the presence of a mass movement unit on the seabed does not necessarily indicate recent emplacement. However, presence below a unit does signify emplacement prior to that of the overlying unit.

From the pinger data analysed, the dating of foraminifera overlying a debrite and analysis of other local chronologies identifies two periods of mass movement on the Barra Fan (see Figure 15 for a stratigraphic overview). The earliest consists of instances of FIV and FV situated below FIIa (see Figure 13c), therefore assumed deposited immediately prior to this overlying unit, and may be estimated to have been emplaced between 21 and 20 ka cal BP.

The second period of mass movement identified is at the termination, or during the final stages, of deposition of FIIa; and prior to the development of contouritic sediments (FI, see Figure 13b) during the Pre-Boreal and Holocene. The dating of planktonic foraminifera in gravity core 56/-10/239, above debris flow deposits (Figure 10, Table 4 and section 4.2.3), yields an age of circa 11.9 ka cal BP. This pre-dates the age of the base of contourite units in nearby cores (see section 4.3.3) by approximately 500 years, though the similarity of these ages provides greater certainty to the age estimate. A calendar age between 12 and 11 ka cal BP can therefore be assigned to instances of FIV and FV situated below FI.

These two periods represent Peach Debrites 3 and 4 as interpreted by Holmes et al. (1998). The earlier event, situated below the hemipelagic unit FII, dated between 21.02 and 20.87 ka cal BP, corresponding to Peach 3 and the more recent event, situated below the contouritic FI, dated between 12 and 11 ka cal BP corresponding to Peach 4.

Figure 15 provides an overview of the basis for this chronology.

5.1.5. Facies VI

Facies VI is interpreted from the pinger record where blanking is interpreted to have been caused by fluid in the sedimentary column. Seismic blanking within the sedimentary column is caused by two primary reasons: high amplitude reflection units (potentially rock,

salt intrusion, coarse sediments or free gas) resulting in reduced signal strength below them in the sedimentary column; and fluid reducing the reflectivity of host sediments. Pore fluid explusion and upward fluid migration is linked to sediment overpressurisation and has previously been observed on the northwest British continental margin (Baltzer et al., 1998; Selby, 1989). Fluid migration may occur diffusely in the sedimentary column or it may be channeled by faults (Reiche et al., 2011; Talukder, 2012). As such, this paper interprets seismic facies VIa (see Figures 5, 8 and 9) as diffuse fluid expulsion; and seismic facies VIb (see Figure 9) as fluid expulsion associated with faulting.

5.2. Episodes of sediment failure, variations in the British-Irish Ice Sheet and changing oceanographic conditions

Holmes et al. (1998) identified four major debrites within the Peach Slide complex. We now consider these events and their relationship to changing oceanographic and sedimentological conditions on the Barra Fan (refer to Figure 16).

The early- to mid-Pleistocene, when Peach 1 is proposed to have occurred, is prior to the focus of this study. However, for completeness we briefly consider this first identified event. Formation of the Barra Fan began around the intra-Pliocene unconformity at 4 ± 0.5 Ma (Dahlgren et al., 2005), timing that is approximately coincidental with the shoaling of the Panama gateway (Haug and Tiedemann, 1998). As such, the North Atlantic thermohaline circulation system should be broadly consistent (allowing for variation associated with glacial cycles) for the duration of fan development; with northward flowing bottom currents at a range of depths.

The major problem when considering Peach 1 is a lack of information, particularly with regards timing. Based on seismo-stratigraphy, Holmes et al. (1998) propose an early- to mid-Pleistocene date as the event precedes the Intra-Pleistocene unconformity at 0.44 Ma (an event marking the beginning of the period of shelf-edge ice). If correct, this provides a potential 2 Ma window of occurrence, too large to allow any detailed discussion of possible contributing factors. It is tempting to suggest it is likely that the event could have occurred later in this period once a critical mass of sediment had deposited possibly tied to increased rates of sedimentation as the Pleistocene glaciations intensified. However, other factors such as gas hydrate dissociation, under-cutting via bottom current erosion or lateral transfer of excess pore fluid pressure from the centre of the Barra Fan could also be involved.

The marine IRD record suggests a Hebrides shelf grounded ice sheet during the Wolstonian glaciation (173 – 128 ka BP) as well as during the Devensian (Hibbert et al., 2010; Scourse et al., 2009). Thermohaline circulation on the Barra Fan and within the Rockall Trough can be expected to display a similar pattern to that of the last glacial period and current inter-glacial period during this later Pleistocene interval as the global drivers (tectonics and global ice remain broadly consistent). As such, it is anticipated to have been sluggish during glacials and stadials and comparatively vigourous during inter-glacial and inter-stadial periods; when a significant amount of across-slope sediment transport is known to occur (Armishaw et al., 2000; Knutz et al., 2002).

Peach 2 is estimated, on the basis of seismo-stratigraphy, to have occurred at 36.5 ka cal BP (Maslin et al., 2004). This places the event in marine isotope stage (MIS) 3, during a phase of BIIS growth. IRD analysis suggests expansion of the BIIS occurred as early as 46 ka BP, with a significant increase at 38.5 ka BP (Peters et al., 2008; Scourse et al., 2009). This is 2 ka prior to the occurrence of Peach 2. There is little detail available concerning ocean circulation in the Rockall Trough during this period, but, on the basis of the evidence summarised in section 2.2, it is anticipated to by sluggish in comparison to the contemporary circulation.

Outlined in section 2.1, the BIIS shelf-edge LGM is thought to have occurred between 29 and 26 ka cal BP (Clark et al., 2012; Scourse et al., 2009). This period is associated with rapid deposition of glacimarine clays and reduced bottom current velocity (Knutz et al., 2002; Lynch-Stieglitz et al., 2007; McManus et al., 2004; Wilson and Austin, 2002). Sedimentation rates in excess of 1 m ka^{-1} are observed in piston core MD95-2006 on the distal fan (Knutz et al., 2002; Wilson and Austin, 2002). This maximum extent is believed to have been relatively short lived, with retreat from the shelf edge occurring from 24 ka cal BP (Scourse et al., 2009) with Tiree exposed at 20.6 ± 1.2 ka cal BP, signifying the deglaciation of the HIS (Small et al., 2017). During this interval the fan would have been subject to rapid sedimentation (calculated on the basis of seismic facies FII's, commonly observed, 20 m thickness and its 8.55 ka deposition duration (maximum age of FII – Maximum age of FI, see section 4.3.3) sedimentation rates on the fan can be calculated as approximately 2.5 m ka^{-1}).

In this period of ice-retreat, as shown by sub-bottom interpretation tied to ^{14}C dates (see Figures 7 and 11) Peach 3 occurred circa 21 ka cal BP. This is following the period of rapid glacimarine sedimentation associated with shelf edge glaciation and Heinrich event 2 and during the deglaciation of the HIS as documented by Small et al. (2017). Glacial

debris flows on the central Barra Fan also occurred during this period and may be coeval with Peach 3. However, the age constraint of these features is less precise as the contourite unit that onlaps Peach 3 in core MD95-2006 is not present on the fan. This means that these debris flow deposits may be estimated to have been emplaced between 18 ka cal BP and 21 ka cal BP.(see Figure 11 and Table 4).

The marine record supports a return to contourite sedimentation immediately after 20.87 ka cal BP (Knutz et al., 2002), however, a return to glacimarine sedimentation follows. Further south, on the flank of Porcupine Seabight, Peck et al. (2007) observe the last significant BIIS input at 16.8 ka cal BP, coeval with Heinrich event 1. Kroon et al. (2000) suggest that the Bølling inter-stadial was fully established by 14.7 ka cal BP, with the Younger Dryas between 13 and 11.0 ka cal BP. The glacial transition was marked by periods of reinvigorated North Atlantic meridional circulation (Thornalley et al., 2010), which would have been associated with increased bottom current vigour and associated sedimentation (Armishaw et al., 2000), as well as colder episodes associated with glacimarine sedimentation (Knutz et al., 2001; Kroon et al., 2000).

Radiocarbon dating of foraminifera in gravity core 56/-10/239 during this study provides a date of 11.9 ka cal BP for sediments that overlie a debrite consisting of full glacial $\delta^{18}O$ material. As shown in Figures 12 and 13, a contourite unit (the base of which is dated at 11.3 ka cal BP; see Figures 14 and 15) drapes the majority of debris flow facies in the Peach Slide area. This observation, combined with the age of foraminifera overlying the debrite in gravity core 56/-10/239, suggests that the Peach 4 event occurred between 12 and 11.0 ka cal BP. This is during the Younger Dryas, with Holocene conditions not fully established on the Barra Fan until 10.9 ka cal BP (Kroon et al., 2000).

There is evidence supporting the presence of a marine terminating ice sheet during the Younger Dryas (Scourse et al., 2009). If, as suggested here, the earlier Peach 3 event occurred at 21 ka cal BP, then 10s of metres of sediment would have accumulated on the upper and middle slopes in the intervening period during the deglaciation.

The occurrence of some mass movement facies exposed on the seabed probably reflects the action of Holocene current scour, though an additional, more recent, failure (supported by the age reversal at 1.57 m in gravity core 56/-10/239) is possible.

Table 6 provides an executive summary of the Peach Debrite ages. It should be noted that the dates of Peach 1, in particular, and Peach 2 are very loosely constrained and more geophysical and sediment core data is required to accurately understand the events. Even the more recent phases of the Peach Slide are associated with a considerable degree of

uncertainty, therefore there is a need for future research designed to improve the constraints on their timing relative to the glacial and deglacial history of the northwest British continental margin.

5.3. Pre-conditioning and potential triggers operating on the Barra Fan and Peach Slide complex

5.3.1. Evidence from the Peach Slide

During inter-glacial periods, the Barra Fan is strongly influenced by across-slope flowing bottom currents, which operate at a range of depths (Figure 1C, Section 2.2). During these periods sedimentation is dominated by hemipelagites and contourites (see section 5.1 and Armishaw et al. (2000), Knutz et al. (2002)). During glacial periods, particularly during the more intense glaciations of the later Pleistocene, sedimentation is dominated by glacimarine processes when the BIIS reached the shelf edge and the Barra Fan was fed by a confluence of ice streams (Clark et al., 2012; Dove et al., 2015; Hibbert et al., 2010; Knutz et al., 2001; Scourse et al., 2009).

Sections 4.1 and 5.1.4 outlines features associated with mass movement mapped within the Peach Slide complex. These include rafted blocks, faults with little vertical displacement, extensional faulting and debris flow deposits. These features appear to support the movement of material in a planar motion. There is also evidence of retrogression, with lower scarps obscured by debris flow deposits from those evacuation areas situated above. Fluid release is also apparent; evidence of this is presented Figures 5 and 6.

This study has also documented preferential accumulation of sediments (interpreted as muddy contourites) within the upper Peach Slide scar (Figure 12), particularly in areas shallower than 1500 m water depth. These accumulations reach a maximum thickness of 9 m, though there is variation with other areas 2 m or less. At greater depths there is no deposition of this unit, with debris flow deposits exposed on the seabed.

This study has focused on the two most recent failures within the Peach Slide complex, Peach 3 and Peach 4, and we have refined and increased the confidence in the age estimates for these two events (outlined in section 5.1.4.3). The chronology of these events in their relation to changes in the BIIS was outlined in section 5.2.

5.3.2. Possible mechanistic analogues from the global submarine mass movement database

We now consider possible analogues for the Peach Slide and Barra Fan, and draw on this wider literature in order to improve understanding of the potential failure mechanisms. Studies on mid- to high-latitude passive continental margin submarine mass movements are largely focused on the northwest European and the eastern North American margins, thus, it is here we focus our attention.

A large number of submarine mass movements are documented on the eastern North American margin and the open slope failures documented here (Chaytor et al., 2009; Twichell et al., 2009) do share morphological similarities with the Peach Slide. However, south of Nova Scotia (where there is no clear analogue for the Peach Slide), there was no shelf-edge ice on the margin, with rivers supplying sediment to shelf-edge deltas instead, with the majority of open slope failures occurring in these areas of thicker Pleistocene and Holocene sediment accumulation (Twichell et al., 2009). Further south there is less of a glacial influence with more pronounced roles played by local factors, such as salt diapirism (Hornbach et al., 2007; Popenoe et al., 1991).

Located within the Rockall Trough, and active during a similar geological period, the Rockall Bank Slide Complex (Georgiopoulou et al., 2013) is geographically the closest large-scale submarine mass movement. However, situated on the sediment-starved Rockall Bank, this event would not seem a close analogue.

As a trough mouth fan, the sediment failures located within the Barra Fan are expected to share more similarities to other such failures, of which there are several on the Norwegian and Barents Sea margins (Vorren and Laberg, 1997). A large number of mass movement events have been documented on these fans, covering a time period from the late-Pliocene (Evans et al., 2005; Safronova et al., 2017) to the Holocene (Laberg et al., 2002a). Frequencies of failure events have increased since shelf-edge glaciation (Safronova et al., 2017; Solheim et al., 2005).

There are similarities in the geological setting of the Barra Fan and the Barents Sea and Norwegian margins: shelf-edge ice, strong across-slope bottom current flow during inter-glacial periods, and a similar tectonic setting on the northwest European rifted margin (though the Barents Sea is tectonically more active with the Mohns and Knipovich ridges (Safronova et al., 2017)). There are also differences in setting, there was more ice located proximal to these more northern depo-centres (Hughes et al., 2016) and thicker accumulations of contourites were deposited during inter-glacial periods (Bryn et al., 2005b). The Hebrides Terrace Seamount is also a key feature that exerts a pronounced

influence on the Barra Fan's sedimentology and has no analogue within the region's trough mouth fans.

It is generally accepted that submarine slope failures require pre-conditioning, or susceptibility, to failure via longer term processes and final triggering via shorter duration events (e.g. Masson et al., 2006; Owen et al., 2007). Pre-conditioning is related to margin evolution, where cyclic sedimentation of contourites and glacigenic material is argued to have played a very strong role on the Norwegian margin creating units with high fluid content that constitute weak layers (Bryn et al., 2005a; Bryn et al., 2005b; Laberg et al., 2003). Isostatic adjustment, with enhanced seismicity and slope steepening has also been identified as an important factor (Bryn et al., 2005a; Laberg and Vorren, 2000). Other studies have also focused on the role of sea level rise, potentially resulting in crustal flexure and faulting (Brothers et al., 2013) and increased sediment pore pressure (Smith et al., 2013).

Creating elevated pore water pressure, as has been suggested by others (e.g. Talling et al., 2014), may be the key to creating the weak layers that allow planar sliding to occur on low angle slopes. Different mechanisms have been invoked to facilitate this process, including rapid sedimentation, gas hydrate dissociation, seismic shaking and lateral pressure transfer. Of the locations discussed here, rapid sedimentation via either fluvial, in the case of the eastern North American margin (Twichell et al., 2009), or glacial, in the case of the northwest European margin (Bryn et al., 2005b; Laberg et al., 2003) is perhaps the most common and plausible. In the case of the Storegga Slide, lateral fluid flow from the North Sea Fan is proposed to have caused liquefaction of sediments lower down the slide, which failed initiating retrogression up the slope (Bryn et al., 2005a; Kvalstad et al., 2005). Gas hydrate dissociation has often been posited (Mienert et al., 1998; e.g. Paull et al., 1996), however, documented slides have generally been initiated at depths lower than the gas hydrate stability zone boundary and gas hydrates are proposed to have had no more than a secondary role in many cases (e.g. Mienert et al., 2005).

5.3.3. Proposed failure mechanism for the Peach Slide

5.3.3.1. Sequence of events

We now consider the morphology of the Peach Slide, its setting and the timing of events in order to propose a failure mechanism for these events.

Timing of Peach 1 is very loosely constrained, but it is proposed to have occurred during the early- to mid-Pleistocene (Holmes et al., 1998). The sedimentology of the fan is

unclear at this time period, though fan progradation commenced at ~4 ± 0.5 Ma and has been linked to increased continental erosion linked to uplift and increased runoff (Dahlgren et al., 2005). Glacial input from the BIIS is first recorded in the Rockall Trough at 2.6 Ma (Thierens et al., 2012) and it seems that the sediments failed once a critical point was reached.

Peach 2, is believed, with some uncertainty, to have occurred at 36.5 ka cal BP during a phase of BIIS expansion into the marine sector. Taken at face value, this provides a period of at least 400 ka for sediment accumulation prior to Peach 2, without any major failure occurring during a number of glacial cycles, where the ice reached the shelf-edge at least once (Hibbert et al., 2010; Stoker, 1995). This is intriguing and constrasts with the three failure events that are proposed to have occurred since 36.5 ka cal BP.

Occurring at circa 21 ka cal BP, towards the end of the deglaciation of the HIS (Small et al., 2017) Peach 3 followed a period that would have been typified by very rapid deposition of clay-rich glacimarine sediments, following the BIIS LGM when it was at the shelf-edge for at least 4 ka. This is approximately 15 ka after the preceding Peach 2, a period marked by the BIIS LGM and glacimarine sedimentation. However, increased bottom current vigour is expected to have occurred during the warmer inter-stadial periods that occurred during this last glacial period. As the BIIS is reconstructed as having retreated some 70 km from the shelf-edge by 21 ka cal BP (Hughes et al., 2016), it is likely that isostatic adjustment had begun prior to the occurrence of Peach 3.

The most recent, and smallest, of the mapped events within the Peach Slide occurred between 11 and 12 ka cal BP, in the later stages of the Younger Dryas. This is approximately 10 ka after the preceding event, Peach 3. This is a period of glacimarine sedimentation (Knutz et al., 2002), sea-level rise and ongoing isostatic rebound (Lambeck, 1995). During the interval between Peach 4 and 3 there were periods of enhanced bottom current circulation as well as rapid deposition of glacimarine sediments during the retreat of the BIIS to an onshore position (Clark et al., 2012; Everest et al., 2006).

5.3.3.2. Failure model

The key factor in slope failure in the Peach Slide seems to be the interaction between sediments deposited via slope-parallel currents and those deposited via downslope glacigenic processes.

In this model, under inter-glacial conditions the vigourous bottom current flow erodes and entrains finer material from the central fan, depositing the sediment within the Peach Slide

scar as the current reduces velocity to due bathymetric interaction with the seabed morphology and Hebrides slope (in a mechanism similar to that proposed by Solheim et al. (2005) at Storegga and by Voigt et al. (2013) for the Plata del Mar canyon). During glacial periods clays would be expected to dominate (deposited from iceberg rainout or turbidity currents via across-slope current transport) and could be deposited extremely rapidly, particularly during the deglaciation.

This process would magnify the glacial to inter-glacial sedimentation cyclicity, with distinct differences between the low-permeability clays, and contourites and hemipelagites with greater water content. During deglacial periods rapid sediment loading would occur as the ice-streams retreated from the shelf-edge, compressing the hemipelagites and contourites below the low permeability glacigenic clays. Such a process would lead to increased pore pressure in the units underlying the glacial material, which could either liquefy and fail directly, or reduce the magnitude of trigger required in order to initiate slope failure.

Based on the timing of the last three large-scale failures within the Peach Slide complex (see Section 5.3.3.1) it seems likely that there is variation in the triggering of these events. However, the pre-conditioning factors appear constant. The mapped accumulation of contourites on the seabed in the slide's scar (Figure 12) and the timing of each event in a period of glacimarine sedimentation support this.

We propose (as Holmes et al. (1998) also commented) that the Hebrides Terrace Seamount plays an important role in at least two ways. First by buttressing the central Barra Fan to the south, and second by funneling the bottom current leading to a potential increase in velocity and, therefore, increased erosion on the central fan.

This seems to make the Peach Slide particularly efficient at generating failures in the last glacial, with three events apparent occurring between 36.5 and 11 ka cal BP. This is distinct from Storegga, which has failed at an approximate 100 ka interval during the late Pleistocene and Holocene (Solheim et al., 2005), though more similar to Trændajupet, which has late glacial and Holocene failures (Laberg et al., 2002a).

The apparent age gap between Peach 1 (likely prior to 0.44 Ma (Holmes et al., 1998)) and Peach 2 (36.5 ka cal BP (Maslin et al., 2004)) is noteworthy and, despite these earlier events not being the focus of this study, requires some discussion. There is a possibility that the age of one or both of these events is incorrect, Peach 1 is more likely to be more erroneous due to the acknowledged loose constraints (Holmes et al., 1998). Peach 3 is dated via seismo-stratigraphy tied to core chronology (work undertaken in constructing the

database used by Maslin et al., 2004), but the event is not well mapped and could be a composite failure.

Another possibility is that sedimentation rates on the Barra Fan were lower prior to the last glacial and that there was insufficient sediment accumulation to pre-condition the slope until the expansion of the BIIS in MIS 3, when Peach 2 occurred. A less pronounced glacial influence on the fan would also reduce the potential frequency of triggering events due to fewer periods of rapid sediment deposition and lower magnitude isostasy. Following Peach 2, rapid sedimentation, associated with the BIIS LGM and subsequent retreat would have contributed to the occurrence of Peach 3, which may have been triggered by a combination of rapid glacimarine sedimentation and isostatic seismicity. Following this, the smaller Peach 4 occurred some 10 ka later, during which interval at least 25 m of sediment (see section 5.2) accumulated, in a period of rising sea-level and elevated isostatic seismicity. A triggering role may also be played by undercutting of sediment via across-slope current erosion, which is observed on the seabed in this area in water depths >1500 m (see Figures 12 and 14A: Knutz et al. (2002)). We speculate that this smaller event may be linked to slope stabilisation following slope steepening associated with Peach 3.

The significant reduction in event volume, as calculated by Holmes et al. (1998), from Peach 1 to Peach 4 supports the above argument. Peach 1, the largest and earliest event (835 km^3), occurs when triggering mechanisms were less frequent, prior to the intensified glaciations, allowing significant sediment accumulation prior to failure. Peach 3, the next most voluminous (673 km^3), occurs several 100 ka later after considerable sediment accumulation during a glacial period. Peach 3 (199 km^3), occurs 15 ka later after a period of rapid sedimentation and was potentially triggered by the HIS collapse. Finally, Peach 4 (135 km^3) occurs 10 ka later and was potentially triggered by some combination of rapid sedimentation, sea-level rise and isostatic seismicity.

6. Conclusions

Two distinct phases of mass movement are identified on the Barra Fan during the late Pleistocene. The first, which includes the Peach 3 event, at circa 21 ka cal BP, shortly after the maximum advance of the BIIS (Knutz et al., 2007; Scourse et al., 2009) and Heinrich event 2 (Hemming, 2004), coeval with the deglaciation of the HIS (Small et al., 2017).

A second phase of mass movement is constrained between 12 and 11 ka cal BP, via ^{14}C dating of planktonic foraminifera in gravity core 56/-10/239 and the onset of contouritic

sedimentation following ice-retreat, at the end of the Younger Dryas stadial. The Peach 4 event is associated with this more recent phase of mass movement. Table 6 provides an overview of the different Peach Debrite ages and their associated uncertainty.

A major finding of this study, shown in Figure 12, is that sediments are preferentially accumulating within the Peach Slide scar. On the basis of seabed morphology, unit asymmetry, seismic facies, the oceanographic setting and previous studies in the region these sediments are interpreted as muddy contourites. Further thick sequences of hemipelagites are also observed on the Barra Fan. Discussed in section 5.3, it is proposed that during periods of ice-retreat the rapid deposition of clay-rich, low-permeability glacigenic sediments on top of contourite and hemipelagite sediments, with a high pore water content, led to development of excess pore pressure. This resulted in reduced sediment shear strength and potential liquefaction.

The timing of Peach 3, at 21 ka cal BP, is coeval with the deglaciation of the HIS and the exposure of Tiree at 20.6 ± 1.2 ka cal BP (Small et al., 2017). This provides strong supporting evidence for failure being initiated via excess pore pressure produced by rapid loading of low permeability glacial clays. Approximately 4 ka after the BIIS maximum extent (Clark et al., 2012; Hughes et al., 2016; Scourse et al., 2009), it is possible that the effects of isostasy played a role in the triggering of this event.

However, based on the timing of Peach 4, between 12 and 11 ka cal BP, an earthquake associated with post-glacial seismicity is possible, as is undercutting via the reinvigourated bottom current flow during the Holocene transition. The rising sea level may also have played a role, either via increased pore pressure (in a mechanism proposed by Smith et al. (2013)), or via crustal flexure and shallow faulting (Brothers et al., 2013).

A further intriguing aspect of the Peach Slide is the large apparent age gap between Peach 1 and Peach 2, based on current dating at least 400 ka, and short intervals between Peach 2 and 4, with the three events occurring in a 25 ka period. This may be due to dating inaccuracies associated with the earlier events, or it could also reflect increased sedimentation rates with the intensification of the Pleistocene glaciations; an intensification that would also have been associated with increased frequency of potential trigger events.

The Peach Slide clearly provides a useful analogy to mass movement events that could be initiated by ongoing deglaciation in Greenland and Antarctica. However, there is still considerable uncertainty concerning the morphology of all the Peach Slide events and the

timing of Peach 1 and 2 and therefore, further studies are required to fully understand the system and how it may relate to the modern context.

Acknowledgements

MO thanks the UCL Graduate School, the ECRC and ENSIS trust fund. NERC funded radiocarbon analysis of core sample 56/-10/239 via allocation number 1441.1009. Doug Masson kindly supplied the NOC geophysical data. DL publishes with permission of the Executive Director, British Geological Survey (NERC). We thank two anonymous reviewers for their constructive comments that have significantly strengthened this paper.

Figure Captions

Figure 1. Regional map showing location of the Barra Fan in relation to major terrestrial and marine features, bathymetric contours (from EMODnet, 2017) at 250 m intervals. A. The Barra Fan in the NE Atlantic Ocean, AD: Anton Dohrn, BF: Barra Fan, DF: Donegal Fan, HTS: Hebrides Terrace Seamount, RB: Rosemary Bank, RT: Rockall Trough, SK: St Kilda. B. Glacial features, dashed blue line indicates maximum extent of BIIS during the LGM with uncertainty in the vicinity of St Kilda (see Clark et al., (2012) and Ballantyne et al., (2017)), thicker dashed lines indicate approximate location of ice-streams (from Bradwell et al., (2008); Dove et al., (2015)), dotted areas indicate location of glacigenic fans, diagonally hatched areas indicate major marine igneous intrusions, and Peach Debrite locations as mapped by Holmes et al., (1998) also shown. C. Oceanographic setting of the Barra Fan, with upper (Holliday et al., 2000; New and Smythe-Wright, 2001), intermediate (Johnson et al., 2010; Ullgren and White, 2010) and deep water flow (New and Smythe-Wright, 2001) shown.

Figure 2. Detailed bathymetry from the Barra Fan region. A. Hebrides and Malin Shelves with deeps (NSD: North Stanton Deep, CSD: Central Stanton Deep, SSD: South Stanton Deep); location of seismic sections in Figures 4 to 8 also shown. B. Detail of LOIS SES multibeam bathymetry from the shelf edge and slope.

Figure 3. Location of sediment core samples, geophysical and bathymetric data in relation to the Barra Fan and Peach Slide. Location of interpreted pinger records in Figures 4 to 8 also shown.

Figure 4. Seismic data example, showing facies Ia (muddy contourite) and facies II (hemipelagite); from BGS pinger record 1985 6-16. VE x 25. Location shown in Figures 2 and 3.

Figure 5. Seismic data example showing facies IVa (high viscosity debris flow deposit) and, with IVc (prominent internal unit); Seismic facies II and Via also interpreted from BGS pinger record 1985 6-13. VE x 8. Location shown in Figures 2 and 3.

Figure 6. Seismic data showing current scour and deposition from pinger line BGS 1985 6-23. Note surface sediments (FI) have been reworked by the prevailing current, which flows south to north. VE x 23. Location shown in Figures 2 and 3.

Figure 7. Seismic data example showing extensional faulting at the slide's northern margin in the lower landslide scar. VE x 9. Location shown in Figures 2 and 3.

Figure 8. Pinger data example from upper landslide scar showing slumped sediments with contourite drift formation. Example from BGS pinger line 1985 6-27, VE × 17. Location shown in Figures 2 and 3.

Figure 9. Overview of interpreted seismic facies, refer to Table 1 and the text for further discussion and evidential support. Note that scales vary on the data examples.

Figure 10. Gravity Core 56/-10/239, A. Core log and uncorrected ^{14}C dates. B. Percentage sand, silt and clay. C. Mean grain size and sorting. D. $\delta^{18}O$ isotope records for planktonic foraminifera *G. bulloides* and *N. pachyderma (s.)*. E. Sedimentation process interpretation.

Figure 11. Radiocarbon chronology and lithology from existing cores in the Peach Slide area. A. Piston core MD95-2006 (uncorrected ^{14}C dates from Knutz et al. (2001) and Austin et al. (2012); lithology and seismic interpretation from Knutz et al. (2002)). B. Vibrocore 56/-10/36, lithology and uncorrected ^{14}C dates from Kroon et al. (1997). C. Locations of cores in relation to Peach Slide.

Figure 12. Thickness of interpreted seismic facies I, shown in relation to the Peach Slide scar.

Figure 13. Distribution of mass movement associated facies. A. At seabed, consisting of deposits from both Peach 3 and Peach 4. B. Below contourite, consisting of deposits from Peach 4. C. Below hemipelagite, consisting of deposits from Peach 3.

Figure 14. Stratigraphic position of debris flow facies from BGS pinger data examples with age constraint. A. Exposed on seabed. B. Below contourite. C. Below hemipelagite.

Figure 15. Chronology of units within the study site. See Table 3 for details of calendar age calculations and text for discussion of seismic facies age.

Figure 16. Schematic of sedimentation driven slope failure on the Barra Fan, with BIIS and ocean circulation. Refer to text for detailed discussion and evidential support.

Table captions

Table 1. Interpreted seismic units, refer also to Figure 5.

Table 2. AMS ^{14}C results from core sample 56/-10/239.

Table 3. Summary of ^{14}C marine reservoir corrections used. Radiocarbon period is reservoir corrected calendar age equivalent from IntCal09 calibration curve (Bronk Ramsey, 2009).

Table 4. Calibration of radiocarbon chronology to calendar years BP. Radiocarbon dates for core sample 56/-10/36 from Kroon et al. (1997) and MD95-2006 from Knutz et al. (2001), Wilson and Austin (2002) and Austin et al. (2012).

Table 5. Age constraint of seismic facies.

Table 6. Executive summary of Peach Debrite ages, supporting evidence and associated uncertainty.

Additional data

Digital Supplement A: AFEN Side scan sonar mosaic and interpretation.

Digital Supplement B: Cross referencing MD95-2006 with BGS seismic data and the seismic interpretation presented in this study.

References

AFEN, 1998. AFEN: UKCS 17th Round Atlantic Margins Environmental Survey. NOC, Southamptom.

Armishaw, J.E., 1999. Bottom current accumulation and sediment fluxes on the Hebridean slope, Geology. University of Southampton, Southampton, p. 215.

Armishaw, J.E., Holmes, R.W., Stow, D.A.V., 1998. Morphology and Sedimentation on the Hebrides slope and Barra Fan, NW UK Continental Margin, in: Stoker, M.S., Evans, D., Cramp, A. (Eds.), Geological Processes on the Continental margins: Sedimentation, Mass-wasting and stability. Geological Society, London, pp. 81-104.

Armishaw, J.E., Holmes, R.W., Stow, D.A.V., 2000. The Barra Fan: A bottom-current reworked, glacially-fed submarine fan system. Marine and Petroleum Geology 17, 219-238.

Austin, W., Hibbert, F., Rasmussen, S.O., Peters, C., Abbott, P., Bryant, C., 2012. The synchronization of palaeoclimatic events in the North Atlantic region during Greenland Stadial 3 (ca 27.5 to 23.3kyr b2k). Quaternary Science Reviews 36, 154-163.

Austin, W.E.N., Bard, E., Hunt, J., Kroon, D., Peacock, J., 1995. The ^{14}C age of the Icelandic Vedde ash: implications for Younger Dryas marine reservoir age corrections. Radiocarbon 37, 53-62.

Austin, W.E.N., Hibbert, F.D., 2012. Tracing time in the ocean: a brief review of chronological constraints (60-8 kyr) on North Atlantic marine event-based stratigraphies. Quaternary Science Reviews 36, 28-37.

Austin, W.E.N., Telford, R.J., Ninnemann, U.S., Brown, L., Wilson, L.J., Small, D.P., Bryant, C.L., 2011. North Atlantic reservoir ages linked to high Younger Dryas atmospheric radiocarbon concentrations. Global And Planetary Change 79, 226-233.

Ballantyne, C.K., Fabel, D., Gheorghiu, D., Rodés, Á., Shanks, R., Xu, S., 2017. Late Quaternary glaciation in the Hebrides sector of the continental shelf: cosmogenic nuclide dating of glacial events on the St Kilda archipelago. Boreas 46, 605-621.

Baltzer, A., Holmes, R., Evans, D., 1998. Debris flows on the Sula Sgeir Fan, NW of Scotland, in: Stoker, M.S., Evans, D., Cramp, A. (Eds.), Geological Processes on Continental Margins: Sedimentation, Mass-Wasting and Stability. Geological Society, London, pp. 105-115.

Bard, E., Arnold, M., Mangerud, J., Paterne, M., Labeyrie, L., Duprat, J., Mélèires, M., Sønstegaard, E., Duplessy, J., 1994. The North Atlantic atmosphere-sea surface ^{14}C gradient during the Younger Dryas climatic event. Earth and Planetary Science Letters 126, 275-287.

Bea, R.G., Wright, S.G., Sircar, P., Niedoroda, A.W., 1983. Wave-Induced Slides in South Pass Block 70, Mississippi Delta. Journal of Geotechnical Engineering 109, 619-644.

Björck, S., Koç, N., Skog, G., 2003. Consistently large marine reservoir ages in the Norwegian Sea during the Last Deglaciation. Quaternary Research, 429-435.

Blott, S., Pye, K., 2001. GRADISTAT: a grain size distribution and statistics package for the analysis of unconsolidated sediments. Earth Surface Processes and Landforms 26, 1237-1248.

BODC, 1999. LOIS Shelf Edge Study Data Set (CD-ROM). British Oceanographic Data Centre.

Bond, G., Broecker, W., Johnsen, S., McManus, J., Labeyrie, L., Jouzel, J., Bonani, G., 1993. Correlations between climate records from North-Atlantic sediments and Greenland ice. Nature 365, 143-147.

Bondevik, S., Lovholt, F., Harbitz, C., Mangerud, J., Dawson, A., Svendsen, J.I., 2005. The Storegga Slide tsunami - comparing field observations with numerical simulations. Marine and Petroleum Geology 22, 195-208.

Bondevik, S., Mangerud, J., Birks, H.H., Gulliksen, S., Reimer, P., 2006. Changes in North Atlantic Radiocarbon Reservoir Ages During the Allerod and Younger Dryas. Science 312, 1514-1517.

Bradwell, T., Stoker, M., Golledge, N., Wilson, C., Merritt, J., Long, D., Everest, J., Hestvik, O., Stevenson, A., Hubbard, A., 2008. The northern sector of the last British Ice Sheet: Maximum extent and demise. Earth-Science Reviews 88, 207-226.

Bronk Ramsey, C., 2009. Bayesian analysis of radiocarbon dates. Radiocarbon 51, 337-360.

Brothers, D.S., Luttrell, K.M., Chaytor, J.D., 2013. Sea-level–induced seismicity and submarine landslide occurrence. Geology 41, 979-982.

Bryn, P., Berg, K., Forsberg, C.F., Solheim, A., Kvalstad, T.J., 2005a. Explaining the Storegga Slide. Marine and Petroleum Geology 22, 11-19.

Bryn, P., Berg, K., Stoker, M.S., Haflidason, H., Solheim, A., 2005b. Contourites and their relevance for mass wasting along the Mid-Norwegian Margin. Marine and Petroleum Geology 22, 85-96.

Bulat, J., Long, D., 2001. Images of the seabed in the Faroe-Shetland Channel from commercial 3D seismic data. Marine Geophysical Researches 22, 345-367.

Bungum, H., Olesen, O., Pascal, C., Gibbons, S., Lindholm, C., Vestol, O., 2010. To what extent is the present seismicity of Norway driven by post-glacial rebound? Journal of the Geological Society 167, 373-384.

Canals, M., Lastras, G., Urgeles, R., Casamor, J., Mienert, J., Cattaneo, A., De Batist, M., Haflidason, H., Imbo, Y., Laberg, J., Locat, J., Long, D., Longva, O., Masson, D., Sultan, N., Trincardi, F., Bryn, P., 2004. Slope failure dynamics and impacts from seafloor and shallow sub-seafloor geophysical data: case studies from the COSTA project. Marine Geology 213, 9-72.

Cao, L., Fairbanks, R.G., Mortlock, R., Risk, M., 2007. Radiocarbon reservoir age of high latitude North Atlantic surface water during the last deglacial. Quaternary Science Reviews 26, 732-742.

Chaytor, J.D., Brink, U., Solow, A.R., Andrews, B.D., 2009. Size distribution of submarine landslides along the U.S. Atlantic margin. Marine Geology 264, 16-27.

Clark, C.D., Hughes, A.L., Greenwood, S.L., Jordan, C., Sejrup, H.P., 2012. Pattern and timing of retreat of the last British-Irish Ice Sheet. Quaternary Science Reviews 44, 112-146.

Coakley, J.P., Syvitski, J.P.M., 1991. SediGraph technique, in: Syvitski, J.P.M. (Ed.), Principles, methods and applications of particle size analysis. Cambridge University Press, Cambridge, pp. 129-142.

Dahlgren, K.I.T., Vorren, T.O., Stoker, M.S., Nielsen, T., Nygard, A., Sejrup, H.P., 2005. Late Cenozoic prograding wedges on the NW European continental margin: their formation and relationship to tectonics and climate. Marine and Petroleum Geology 22, 1089-1110.

Damuth, J.E., 1978. Echo character of the Norwegian--Greenland Sea: relationship to Quaternary sedimentation. Marine Geology 28, 1-36.

Damuth, J.E., Jacobi, R.D., Hayes, D.E., 1983. Sedimentation processes in the Northwest Pacific Basin revealed by echo-character mapping studies. Geological Society of America Bulletin 94, 381-395.

Davies, S., Wastegård, S., Rasmussen, T., Svensson, A., Johnsen, S., Steffensen, J., Andersen, K., 2008. Identification of the Fugloyarbanki tephra in the NGRIP ice core: a key tie-point for marine and ice-core sequences during the last glacial period. Journal of Quaternary Science 23, 409-414.

Dickson, R.R., McCave, I.N., 1986. Nepheloid layers on the continental-slope west of Porcupine Bank. Deep-Sea Research Part A-Oceanographic Research Papers 33, 791-818.

Dorn, W., Werner, F., 1993. The contour-current flow along the southern Iceland-Faeroe Ridge as documented by its bedforms and asymmetrical channel fillings. Sedimentary Geology 82, 47-59.

Dove, D., Arosio, R., Finlayson, A., Bradwell, T., Howe, J.A., 2015. Submarine glacial landforms record Late Pleistocene ice-sheet dynamics, Inner Hebrides, Scotland. Quaternary Science Reviews 123, 24.

Dunlop, P., Shannon, R., McCabe, M., Quinn, R., Doyle, E., 2010. Marine geophysical evidence for ice sheet extension and recession on the Malin Shelf: New evidence for the western limits of the British Irish Ice Sheet. Marine Geology 276, 86-99.

EMODnet, 2017. Bathymetry Portal.

Evans, D., Harrison, Z., Shannon, P.M., Laberg, J.S., Nielsen, T., Ayers, S., Holmes, R., Hoult, R.J., Lindberg, B., Haflidason, H., Long, D., Kuijers, A., Andersen, E.S., Bryn, P., 2005. Palaeoslides and other mass failures of Pliocene to Pleistocene age along the Atlantic continental margin of NW Europe. Marine and Petroleum Geology 22, 1131-1148.

Evans, D., Kenolty, N., Dobson, M.R., Whittington, R.J., Durant, G.P., Barber, P., 1983. Malin. Sheet 55°N - 08°W. Solid Geology., 1:250 000 series. British Geological Survey.

Everest, J.D., Bradwell, T., Fogwill, C.J., Kubik, W., 2006. Cosmogenic ^{10}Be age constraints for the Wester Ross readvance moraine: Insights into British ice-sheet behaviour. Geografiska Annaler 88 A, 9 - 17.

Fairbanks, R., Mortlock, R., Chiu, T., Cao, L., Kaplan, A., Guilderson, T., Fairbanks, T., Bloom, A., Grootes, P., Nadeau, M., 2005. Radiocarbon calibration curve spanning 0 to 50,000 years BP based on paired Th/U/U and C dates on pristine corals. Quaternary Science Reviews 24, 1781-1796.

Finlayson, A., Fabel, D., Bradwell, T., Sugden, D., 2014. Growth and decay of a marine terminating sector of the last British-Irish Ice Sheet: a geomorphological reconstruction. Quaternary Science Reviews 83, 18.

Franke, J., Paul, A., Schulz, M., 2008. Modeling variations of marine reservoir ages during the last 45 000 years. Climate Of The Past 4, 125-136.

Georgiopoulou, A., Shannon, P.M., Sacchetti, F., Haughton, P.D.W., Benetti, S., 2013. Basement-controlled multiple slope collapses, Rockall Bank Slide Complex, NE Atlantic. Marine Geology 336, 198-214.

Hall, I., Colmenero-Hidalgo, E., Zahn, R., Peck, V., Hemming, S., 2011. Centennial- to millennial-scale ice-ocean interactions in the subpolar northeast Atlantic 18-41 kyr ago. Paleoceanography 26, n/a-n/a.

Haug, G.H., Tiedemann, R., 1998. Effect of the formation of the Isthmus of Panama on Atlantic Ocean thermohaline circulation. Nature 393, 673-676.

Hemming, S., 2004. Heinrich events: Massive late Pleistocene detritus layers of the North Atlantic and their global climate imprint. Reviews of Geophysics 42, RG1005.

Hibbert, F.D., Austin, W., Lenc, M.J., Gatliff, R.W., 2010. British Ice Sheet dynamics inferred from North Atlantic ice-rafted debris records spanning the last 175 000 years. Journal of Quaternary Science 25, 461-482.

Hiemstra, J.F., Shakesby, R.A., Vieli, A., 2015. Late Quaternary glaciation in the Hebrides sector of the continental shelf: was St Kilda overrun by the British-Irish Ice Sheet? Boreas 22, 19.

Holliday, N.P., Pollard, R.T., Read, J.F., Leach, H., 2000. Water mass properties and fluxes in the Rockall Trough, 1975-1998. Deep-Sea Research Part I-Oceanographic Research Papers 47, 1303-1332.

Holmes, R.W., Long, D., Dodd, L.R., 1998. Large-scale debrites and submarine landslides on the Barra Fan, west of Britain, in: Stoker, M.S., Evans, D., Cramp, A. (Eds.), Geological processes on continental margins: sedimentation, mass wasting and stability. Geological Society, London, pp. 67-79.

Hornbach, M., Lavier, L., Ruppel, C., 2007. Triggering mechanism and tsunamogenic potential of the Cape Fear Slide complex, U.S. Atlantic margin. Geochemistry Geophysics Geosystems 8, 16.

Howe, J.A., 1996. Turbidite and contourite sediment waves in the northern Rockall Trough, North Atlantic Ocean. Sedimentology 43, 219-234.

Howe, J.A., Dove, D., Bradwell, T., Gafeira, J., 2012. Submarine geomorphology and glacial history of the Sea of the Hebrides, UK. Marine Geology 315-318, 64-76.

Hsu, S., Kuo, J., Lo, C., Tsai, C., Doo, W., Ku, C., Sibuet, J., 2008. Turbidity Currents, Submarine Landslides and the 2006 Pingtung Earthquake off SW Taiwan. Terrestrial Atmospheric And Oceanic Sciences 19, 767-772.

Hughen, K.A., Baillie, M.G.L., Bard, E., Beck, J.W., Bertrand, C.J.H., Blackwell, P.G., Buck, C.E., Burr, G.S., Cutler, K.B., Damon, P.E., Edwards, R.L., Fairbanks, R.G., Friedrich, M., Guilderson, T.P., Kromer, B., McCormac, G., Manning, S., Ramsey, C.B., Reimer, P.J., Reimer, R.W., Remmele, S., Southon, J.R., Stuiver, M., Talamo, S., Taylor, F.W., Plicht, J., Weyhenmeyer, C.E., 2004. MARINE04 marine radiocarbon age calibration, 0-26 cal kyr BP. Radiocarbon 46, 1059-1086.

Hughes, A.L.C., Gyllencreutz, R., Lohne, Ø.S., Mangerud, J., Svendsen, J.I., 2016. The last Eurasian ice sheets – a chronological database and time-slice reconstruction, DATED-1. Boreas 45, 45.

IPCC, 2013. Climate Change 2013: The Physical Science Basis. Contribution of Working Group I to the Fifth Assessment Report of the Intergovernmental Panel on Climate Change Cambridge University Press, Cambridge.

Jenner, K.A., Piper, D.J.W., Campbell, D.C., Mosher, D.C., 2007. Lithofacies and origin of late Quaternary mass transport deposits in submarine canyons, central Scotian Slope, Canada. Sedimentology 54, 19-38.

Johnson, C., Sherwin, T., Smythe-Wright, D., Shimmield, T., Turrell, W., 2010. Wyville Thomson Ridge Overflow Water: Spatial and temporal distribution in the Rockall Trough. Deep-Sea Research Part I-Oceanographic Research Papers 57, 1153-1162.

Kennett, J.P., Cannariato, K.G., Hendy, I.L., Behl, R.J., 2003. Methane hydrates in Quaternary climate change: the clathrate gun hypothesis. American Geophysical Union, Washington, D.C.

Knutz, P.C., Austin, W.E.N., Jones, E.J.W., 2001. Millenial-scale depositional cycles related to British Ice Sheet variability and North Atlantic paleocirculation since 45 kyr B.P., Barra Fan, U.K. margin. Paleoceanography 16, 53-64.

Knutz, P.C., Jones, E.J.W., Austin, W.E.N., van Weering, T.C.E., 2002. Glacimarine slope sedimentation, contourite drifts and bottom current pathways on the Barra Fan, UK North Atlantic margin. Marine Geology 188, 129-146.

Knutz, P.C., Zahn, R., Hall, I.R., 2007. Centennial-scale variability of the British Ice Sheet: Implications for climate forcing and Atlantic meridional overturning circulation during the last deglaciation. Paleoceanography 22, 14.

Kohfeld, K., Fairbanks, R., Smith, S., Walsh, I., 1996. Neogloboquadrina pachyderma (sinistral coiling) as paleoceanographic tracers in polar oceans: Evidence from Northeast Water Polynya plankton tows, sediment traps, and surface sediments. Paleoceanography 11, 679-699.

Kroon, D., Austin, W.E.N., Chapman, M.R., Ganssen, G.M., 1997. Deglacial surface circulation changes in the northeastern Atlantic: Temperature and salinity records of NW Scotland on a century scale. Paleoceanography 12, 755 - 763.

Kroon, D., Shimmield, G., Austin, W.E.N., Derrick, S., Knutz, P., Shimmield, T., 2000. Century- to millenial-scale sedimentological-geochemical records of glacial-Holocene sediment variations from the Barra Fan (NE Atlantic). Journal of the Geological Society, London 157, 643-653.

Kvalstad, T.J., Andresen, L., Forsberg, C.F., Berg, K., Bryn, P., Wangen, M., 2005. The Storegga slide: evaluation of trigger sources and slide mechanics. Marine and Petroleum Geology 22.

Laberg, J., Vorren, T., Mienert, J., Bryn, P., Lien, R., 2002a. The Trænadjupet Slide: a large slope failure affecting the continental margin of Norway 4,000 years ago. Geo-Marine Letters 22, 19-24.

Laberg, J.S., Vorren, T.O., 2000. Trænadjupet slide, offshore Norway - morphology, evacuation and triggering mechanisms. Marine Geology 171, 95-114.

Laberg, J.S., Vorren, T.O., Mienert, J., Evans, D., Lindberg, B., Ottesen, D., Kenyon, N.H., Henriksen, S., 2002b. Late Quaternary palaeoenvironment and chronology in the Trænadjupet Slide area offshore Norway. Marine Geology 188, 35-60.

Laberg, J.S., Vorren, T.O., Mienert, J., Haflidason, H., Bryn, P., Lien, R., 2003. Preconditions leading to the Holocene Trænadjupet slide offshore Norway, in: Locat, J., Mienert, J. (Eds.), Advances in Natural and Technological Hazards research. Kluwer, Dordrecht, pp. 247-254.

Lambeck, K., 1995. Glacial isostasy and water depths in the late Devensian and Holocene on the Scottish Shelf west of the Outer Hebrides. Journal of Quaternary Science 10, 83-86.

Lee, H.J., 2009. Timing of occurrence of large submarine landslides on the Atlantic Ocean margin. Marine Geology 264, 53-64.

Lindsey, J., 1989. The Fresnel zone and its interpretive significance. The Leading Edge 8, 33-39.

Lynch-Stieglitz, J., Adkins, J.F., Curry, W.B., Dokken, T., Hall, I., Herguera, J.C., Hirschi, J.J., Ivanova, E.V., Kissel, C., Marchal, O., Marchitto, T.M., McCave, I.N., McManus, J.F., Mulitza, S., Ninnemann, U., Peeters, F., Yu, E., Zahn, R., 2007. Atlantic meridional overturning circulation during the Last Glacial Maximum. Science 316, 66-69.

Marani, M., Argnani, A., Roveri, M., Trincardi, F., 1993. Sediment drifts and erosional surfaces in the central Mediterranean: seismic evidence of bottom-current activity. Sedimentary Geology 82, 207-220.

Maslin, M., Owen, M., Day, S., Long, D., 2004. Linking continental-slope failures and climate change: Testing the clathrate gun hypothesis. Geology 32, 53.

Masson, D.G., Harbitz, C.B., Wynn, R.B., Pedersen, G., Løvholt, F., 2006. Submarine landslides: processes, triggers and hazard prediction. Philosophical Transactions of the Royal Society A: Mathematical, Physical and Engineering Sciences 364, 2009-2039.

Masson, D.G., Jacobs, C.L., 1998. Southampton Oceanography Centre Cruise Report: R.V.Colonel Templer Cruises 01 and 02/98. TOBI surveys of the continental slope north and west of Scotland., Southampton, p. 50.

McCave, I.N., Manighetti, B., Beveridge, N.A.S., 1995. Circulation in the glacial North-Atlantic inferred from grain-size measurements. Nature 374, 149-152.

McManus, J.F., Francois, R., Gherardi, J.M., Keigwin, L.D., Brown-Leger, S., 2004. Collapse and rapid resumption of Atlantic meridional circulation linked to deglacial climate changes. Nature 428, 834-837.

Mienert, J., Posewang, J., Baumann, M., 1998. Gas hydrates along the northeastern Atlantic margin: possible hydrate-bound margin instabilities and possible release of methane, in: Henriet, J.-P., Mienert, J. (Eds.), Gas Hydrates: Relevance to World Margin Stability and Climate Change. Geological Society, London, London.

Mienert, J., Vanneste, M., Bünz, S., Andreassen, K., Haflidason, H., 2005. Ocean warming and gas hydrate stability on the mid-Norwegian margin at the Storegga Slide. Marine and Petroleum Geology 22, 233-244.

New, A.L., Smythe-Wright, D., 2001. Aspects of the circulation in the Rockall Trough. Continental Shelf Research 21, 777-810.

Ó Cofaigh, C., Dunlop, P., Benetti, S., 2012. Marine geophysical evidence for Late Pleistocene ice sheet extent and recession off northwest Ireland. Quaternary Science Reviews 44, 147-159.

Øvrebø, L.K., Haughton, P.D.W., Shannon, P.M., 2006. A record of fluctuating bottom currents on the slopes west of the Porcupine Bank, offshore Ireland - implications for Late Quaternary climate forcing. Marine Geology 225, 279-309.

Owen, M., Day, S., Long, D., Maslin, M., 2010. Investigations on the Peach 4 Debrite, a Late Pleistocene Mass Movement on the Northwest British Continental Margin, in: Mosher, D.C., Shipp, R.C., Moscardelli, L., Chaytor, J.D., Baxter, C.D.P., Lee, H.J., Urgeles, R. (Eds.), Submarine mass movements and their consequences. Springer, Dordrecht, pp. 301-311.

Owen, M., Day, S., Maslin, M., 2007. Late Pleistocene submarine mass movements: occurrence and causes. Quaternary Science Reviews 26, 958-978.

Owen, M.J., 2013. Morphology and timing of submarine mass movement on the northwest British continental margin, Geography. Unpublished Ph.D Thesis UCL, London, p. 267.

Owen, M.J., Maslin, M.A., Day, S.J., Long, D., 2015. Testing the reliability of paper seismic record to SEGY conversion on the surface and shallow sub-surface geology of the Barra Fan (NE Atlantic Ocean). Marine and Petroleum Geology 61, 69-81.

Paull, C.K., Buelow, W.J., Ussler III, W., Borowski, W.S., 1996. Increased continental-margin slumping frequency during sea-level lowstands above gas hydrate-bearing sediments. Geology 24, 143-146.

Peck, V., Hall, I., Zahn, R., Grousset, F., Hemming, S., Scourse, J., 2007. The relationship of Heinrich events and their European precursors over the past 60ka BP: a multi-proxy ice-rafted debris provenance study in the North East Atlantic. Quaternary Science Reviews 26, 862-875.

Peck, V.L., Hall, I.R., Zahn, R., Elderfield, H., 2008. Millennial-scale surface and subsurface paleothermometry from the northeast Atlantic, 55–8 ka BP. Paleoceanography 23, 1-11.

Peters, C., Walden, J., Austin, W., 2008. Magnetic signature of European margin sediments: Provenance of ice-rafted debris and the climatic response of the British ice sheet during Marine Isotope Stages 2 and 3. Journal of Geophysical Research 113, F03007.

Piper, D.J.W., Hiscott, R.N., Normark, W.R., 1999. Outcrop-scale acoustic facies analysis and latest Quaternary development of Hueneme and Dume submarine fans, offshore California. Sedimentology 46, 47-78.

Popenoe, P., Schmuck, E.A., Dillon, W.P., 1991. The Cape Fear landslide: slope failure associated with salt diapirism and gas hydrate decomposition. USGS Bulletin 2002, 40-53.

Praeg, D., Stoker, M.S., Shannon, P.M., Ceramicola, S., Hjelstuen, B., Laberg, J.S., Mathiesen, A., 2005. Episodic Cenozoic tectonism and the development of the NW European 'passive' continental margin. Marine and Petroleum Geology 22, 1007-1030.

Rebesco, M., Stow, D., 2001. Seismic expression of contourites and related deposits: a preface. Marine Geophysical Researches 22, 303-308.

Reiche, S., Hjelstuen, B.O., Haflidason, H., 2011. High-resolution seismic stratigraphy, sedimentary processes and the origin of seabed cracks and pockmarks at Nyegga, mid-Norwegian margin. Marine Geology 284, 28-39.

Safronova, P.A., Laberg, J.S., Andreassen, K., Shlykova, V., Vorren, T.O., Chernikov, S., 2017. Late Pliocene-early Pleistocene deep-sea basin sedimentation at high-latitudes: mega-scale submarine slides of the north-western Barents Sea margin prior to the shelf-edge glaciations. Basin Research 29, 537-555.

Schiebel, R., Bijma, J., Hemleben, C., 1997. Population dynamics of the planktic foraminifer Globigerina bulloides from the eastern North Atlantic. Deep-Sea Research Part I 44, 1701-1713.

Scourse, J.D., Haapaniemi, A.I., Colmenero-Hidalgo, E., Peck, V.L., Hall, I.R., Austin, W.E., Knutz, P.C., Zahn, R., 2009. Growth, dynamics and deglaciation of the last British-Irish ice sheet: the deep-sea ice-rafted detritus record. Quaternary Science Reviews 28, 3066-3084.

Selby, I.C., 1989. The Quaternary Geology of the Hebridean Continental Margin. Unpublished Ph.D Thesis University of Nottingham, Nottingham.

Small, D., Benetti, S., Dove, D., Ballantyne, C.K., Fabel, D., Clark, C.D., Gheorghiu, D.M., Newall, J., Xu, S., 2017. Cosmogenic exposure age constraints on deglaciation and flow behaviour of a marine-based ice stream in western Scotland, 21–16 ka. Quaternary Science Reviews 167, 30-46.

Small, D., Rinterknecht, V., Austin, W.E.N., Bates, R., Benn, D.I., Scourse, J.D., Bourles, D.L., Team, A., Hibbert, F.D., 2016. Implications of ^{36}Cl exposure ages from Skye, northwest Scotland for the timing of ice stream deglaciation and deglacial ice dynamics. Quaternary Science Reviews 150, 16.

Smith, D.E., Harrison, S., Jordan, J.T., 2013. Sea level rise and submarine mass failures on open continental margins. Quaternary Science Reviews 82, 93-103.

Solheim, A., Bryn, P., Sejrup, H.P., Mienert, J., Berg, K., 2005. Ormen Lange - an integrated study for the safe development of a deep-water gas field within the Storegga Slide Complex, NE Atlantic continental margin; executive summary. Marine and Petroleum Geology 22, 1-9.

Stoker, M.S., 1995. The influence of glacigenic sedimentation on slope-apron development on the continental margin off Northwest Britain, in: Scrutton, R.A., Stoker, M.S., Shimmield, G.B., Tudhope, A.W. (Ed.), The Tectonics, Sedimentation and Palaeoceanography of the North Atlantic Region. Geological Society, London, pp. 159-177.

Stoker, M.S., Hitchen, K., Graham, C.C., 1993. The Geology of the Hebrides and the West Shetland shelves, and adjacent deep-water areas, United Kingdom Offshore Regional Report. British Geological Survey, London, p. 149.

Stoker, M.S., Holford, S.P., Hillis, R.R., Green, P.F., Duddy, I.R., 2010. Cenozoic post-rift sedimentation off northwest Britain: Recording the detritus of episodic uplift on a passive continental margin. Geology 38, 595-598.

Stoker, M.S., Hoult, R.J., Nielsen, T., Hjelstuen, B.O., Laberg, J.S., Shannon, P.M., Praeg, D., Mathiesen, A., van Weering, T.C.E., McDonnell, A., 2005a. Sedimentary and oceanographic responses to early Neogene compression on the NW European margin. Marine and Petroleum Geology 22, 1031-1044.

Stoker, M.S., Leslie, A.B., Scott, W.D., Briden, J.C., Hine, N.M., Harland, R., Wilkinson, I.P., Evans, D., Ardus, D.A., 1994. A record of late Cenozoic stratigraphy, sedimentation and climate change from the Hebrides Slope, NE Atlantic Ocean. Journal of the Geological Society 151, 235-249.

Stoker, M.S., Praeg, D., Hjelstuen, B.O., Laberg, J.S., Nielsen, T., Shannon, P.M., 2005b. Neogene stratigraphy and the sedimentary and oceanographic development of the NW European Atlantic margin. Marine and Petroleum Geology 22, 977-1005.

Stow, D.A.V., Faugères, J.-C., 2008. Contourite facies and the facies model, in: Rebesco, M., Camerlenghi, A. (Eds.), Contourites. Elsevier, Amsterdam, pp. 223-255.

Talling, P., Clare, M., Urlaub, M., Pope, E., Hunt, J., Watt, S., 2014. Large Submarine Landslides on Continental Slopes: Geohazards, Methane Release, and Climate Change. Oceanography 27, 32-45.

Talukder, A., 2012. Review of submarine cold seep plumbing systems: leakage to seepage and venting. Terra Nova 24, 255-272.

ten Brink, U.S., Barkan, R., Andrews, B.D., Chaytor, J.D., 2009. Size distributions and failure initiation of submarine and subaerial landslides. Earth and Planetary Science Letters 287, 31-42.

Thierens, M., Pirlet, H., Colin, C., Latruwe, K., Vanhaecke, F., Lee, J.R., Stuut, J.B., Titschack, J., Huvenne, V.A.I., Dorschel, B., Wheeler, A.J., Henriet, J.P., 2012. Ice-rafting from the British–Irish ice sheet since the earliest Pleistocene (2.6 million years ago):

implications for long-term mid-latitudinal ice-sheet growth in the North Atlantic region. Quaternary Science Reviews 44, 229-240.

Thornalley, D.J.R., Elderfield, H., McCave, I.N., 2010. Intermediate and deep water paleoceanography of the northern North Atlantic over the past 21,000 years. Paleoceanography 25, PA1211.

Tripsanas, E., Piper, D., Campbell, D., 2008. Evolution and depositional structure of earthquake-induced mass movements and gravity flows: Southwest Orphan Basin, Labrador Sea. Marine and Petroleum Geology 25, 645-662.

Tripsanas, E.K., Piper, D.J.W., Jenner, K.A., Bryant, W.R., 2007. Submarine mass-transport facies: new perspectives on flow processes from cores on the eastern North American margin. Sedimentology 55, 97-136.

Twichell, D.C., Chaytor, J.D., Brink, U., Buczkowski, B., 2009. Morphology of late Quaternary submarine landslides along the U.S. Atlantic continental margin. Marine Geology 264, 4-15.

Ullgren, J.E., White, M., 2010. Water mass interaction at intermediate depths in the southern Rockall Trough, northeastern North Atlantic. Deep-Sea Research Part I-Oceanographic Research Papers 57, 248-257.

Urlaub, M., Talling, P., Masson, D.G., 2013. Timing and frequency of large submarine landslides: implications for understanding triggers and future geohazard. Quaternary Science Reviews 72, 63-82.

Voigt, I., Henrich, R., Preu, B.M., Piola, A.R., Hanebuth, T.J., Schwenk, T., Chiessi, C.M., 2013. A submarine canyon as a climate archive - Interaction of the Antarctic Intermediate Water with the Mar del Plata Canyon (Southwest Atlantic). Marine Geology 341, 46-57.

Vorren, T.O., Laberg, J.S., 1997. Trough Mouth Fans - Palaeoclimate and Ice-Sheet Monitors. Quaternary Science Reviews 16, 865-881.

Wilson, L., Austin, W., 2002. Millennial and sub-millennial-scale variability in sediment colour from the Barra Fan, NW Scotland: implications for British ice sheet dynamics. Geological Society, London, Special Publications 203, 349-365.

Table 1

Facies	Characteristics visible in Seismic record	Interpretation	Evidential support
Ia	Uppermost unit – Low amplitude and transparent	Muddy contourite	Sampled by BGS core samples and interpreted by Armishaw (1999), Armishaw et al. (2000), Kroon et al. (1997; 2000) and Knutz et al. (2002).
Ib	Uppermost unit – High amplitude	Sandy contourite	
IIa	Parallel reflectors draping underlying units	Hemipelagic sedimentation, consisting of varying contributions from hemipelagic, contouritic, glacigenic and turbiditic sources	Corresponds to the Gwaleo sequence (Stoker et al., 1993). Lack of ground truthing prevents differentiation of sources, which Howe (1996), Kroon et al. (2000) and Knutz et al. (2002) demonstrates are mixed. FIIb represents interpretation of Upper Macleod sequence.
IIb	Unit of parallel reflectors underlaying chaotic or high amplitude facies	Hemipelagic sedimentation, separate facies to simplify analysis	
III	High-amplitude unit	Unit consisting of coarser sediments, which may be sandy contourite or turbidite when ponded	Coarser material provides higher amplitude returns and literature (Howe, 1996; Knutz et al., 2002) supports presence of contourites and turbidites.
IVa	Chaotic, semi-transparent unit with hyperbolae; displaying mounded morphology at upper boundary	High viscosity cohesive debris flow	Chaotic, semi-transparent to transparent facies indicative of debris flow deposits (numerous studies, including Canals et al., 2004; Tripsanas et al., 2007). Higher viscosity results in deposits displaying positive relief, low viscosity materials act more like liquids and infill resulting in zero or negative relief (Tripsanas et al., 2007).
IVb	Chaotic, semi-transparent unit displaying flat to concave upper boundary	Low viscosity cohesive debris flow	
IVc	Prominent reflector within chaotic, semi-transparent unit	Indicating multistage event	
V	High-amplitude, irregular, hyperbolic return	Hard debris	Indication of rugged terrain, noted by numerous studies, including Armishaw et al. (1998), since Damuth et al. (1983).
Via	Seismic blanking within sedimentary column – diffuse	Diffuse fluid escape	Documented on the Sula Sgeir Fan by Baltzer et al. (1998).
VIb	Seismic blanking within sedimentary column - associated fault	Fluid escape associated with polygonal fault	As documented in the Faeroe-Shetland Channel (Bulat and Long, 2001) and Norwegian Margin (Reiche et al., 2011).
VII	Marked reflector displacement or high amplitude vertical reflections below depression	Fault	Diameter of Fresnel zone (see Lindsey, 1989) may obscure detail in deep water and faults are visible as high-amplitude, linear, near-vertical features.

Table 2

Sample number	Sample depth (cm)	Foraminiferal species	14C Enrichment (% Modern ± σ)	Conventional radiocarbon age (years BP ± σ)	±	Carbon content (% by weight)	$\delta^{13}C$ VPDB ± 0.1 ‰
SUERC-28178	16 - 18	*N. pachyderma (s.)*	25.12 ± 0.13	11098	41	10.7	insufficient material
SUERC-28179	156 - 158	*G. bulloides*	20.10 ± 0.11	12889	43	8.6	insufficient material
SUERC-28180	196 - 198	*N. pachyderma (s.)*	26.43 ± 0.14	10688	44	10.5	insufficient material
SUERC-30290	194 - 198	*N. pachyderma (s.)*	25.01 ± 0.13	11134	41	12	-0.4

Table 3

Time period (calendar years)	Time period (name)	Reservoir correction (years)	Corresponding uncorrected ^{14}C period (^{14}C years)	Evidential support
10,000 to present	Holocene	450	9318 to present	General agreement among records and reflects pre-bomb values (Bard et al., 1994).
11,499 to 10,000	Pre-Boreal	400	10400 to 9319	Agreement between Austin et al. (2011) and Bondevik et al. (2006).
12,999 to 11,500	Younger Dryas	700	11795 to 10401	Based on Vedde Ash layer identified within CS 56/-10/36 (Austin et al., 1995) and all other records support elevated values.
14,999 to 13,000	Bølling-Allerød	500	13109 to 11796	Disagreement among records, have opted for a mid-way point between Bondevik et al. (2006) and Austin et al. (2011). Reduced correction compared to adjacent periods is logical due to probable enhanced thermohaline circulation.
20,999 to 15,000	Late Glacial – MIS 2	550	18084 to 13110	High degree of uncertainty due to lack of data. This value is chosen due to modeled value from Franke et al. (2008).
28,500 to 21,000	Late Glacial – MIS 2	950	24710 to 18085	High degree of uncertainty due to lack of data. This value is chosen due to apparent 950 year offset of Fugloyarbanki tephra layer in MD95-2006 (see Davies et al., 2008; Austin et al., 2012; Owen, 2013).

Table 4

Core sample	Depth (m)	Material	Age (Uncorrected ^{14}C BP)	Reservoir correction	Age (calendar years BP - IntCal09)
56/-10/239	0.170	*N. pachyderma (s.)*	11098 ± 41	700	12300 ± 214
56/-10/239	1.570	*G. bulloides*	12889 ± 43	500	14513 ± 413
56/-10/239	1.960	*N. pachyderma (s.)*	11134 ± 41	700	12323 ± 206
56/-10/239	1.970	*N. pachyderma (s.)*	10688 ± 44	700	11482 ± 219
56/-10/239	1.96 and 1.97 combined		10711 ± 43	700	11919 ± 160
56/-10/36	0.725	*G. bulloides*	10040 ± 80	400	10976 ± 230
56/-10/36	0.755	*N. pachyderma (s.)*	10585 ± 85	700	11438 ± 265
56/-10/36	1.245	Vedde Ash	10939	700	11953 ± 116
56/-10/36	2.780	1 Thol. 2 Ash	11293	700	12585 ± 44
56/-10/36	3.550	*G. bulloides*	12055 ± 100	500	13445 ± 230
56/-10/36	4.315	*G. bulloides*	13020 ± 115	500	14643 ± 492
MD95-2006	0.500	G. bulloides	2799 ± 44	450	2434 ± 249
MD95-2006	1.645	G. bulloides	10270 ± 44	400	11298 ± 92
MD95-2006	2.600	1 Thol 2 Ash	11293	700	12585 ± 44
MD95-2006	3.230	*G. bulloides*	11960 ± 120	500	13356 ± 248
MD95-2006	7.600	*N. pachyderma (s.)*	15260 ± 140	550	17999 ± 514
MD95-2006	11.755	*N. pachyderma (s.)*	17390 ± 190	550	19951 ± 466
MD95-2006	13.200	*N. pachyderma (s.)*	18060 ± 130	550	20866 ± 464
MD95-2006	14.110	*N. pachyderma (s.)*	18680 ±130	950	21018 ± 474
MD95-2006	15.915	*N. pachyderma (s.)*	20390 ± 150	950	23138 ± 533
MD95-2006	19.145	*N. pachyderma (s.)*	22720 ± 130	950	26216 ± 519
MD95-2006	19.900	*N. pachyderma (s.)*	24710 ± 280	950	28642 ± 666
MD95-2006	20.105	*G. bulloides*	24571 ± 185	950	28402 ± 503
MD95-2006	20.205	*N. pachyderma (s.)*	24710 ± 280	950	28642 ± 666

Table 5

Facies	Interpretation of facies	Age constraint from core sample	Calendar age (BP) and sample location within core unit	Comment
I	Contourite	MD95-2006 56/-10/36 MD95-2006	2434 ± 249 (mid unit) 11438 ± 265 (base of unit) 11298 ± 92 (base of unit)	
IV (upper unit)	Peach 4 debrite	56/-10/239	11919 ± 160 (base of overlying unit)	Underlies, and is therefore older than, Facies I.
II	Hemipelagite	MD95-2006	17999 ± 514 (mid unit) 19951 ± 466 (top of underlying unit)	
IV (lower unit)	Peach 3 debrite	MD95-2006	20866 ± 464 (base of overlying contourite unit) 21018 ± 474 (top of underlying unit)	Underlies, and is therefore older than, Facies II. Additional contourite unit interpreted by Knutz et al. (2002), dated by Wilson and Austin (2002) further constrains the age.

Table 6

Event	Age	Basis and uncertainty	References
Peach 4	11 - 12 ka cal BP	Sediments overlying debris flow deposit in core sample 56/-10/239 dated at 11.9 ± 0.16 ka cal BP. Base of contourite unit, that overlies debrite, dated at 11.4 ka cal BP. Core sample 56/-10/239 is subject to an age reversal and does not represent continual sedimentation. A hiatus could be present between deglacial and contouritic sedimentation. Analysis of additional core samples that overlie and penetrate the event is needed is improve certainty.	This paper, Owen (2013).
Peach 3	21 ka cal BP	Sediments that onlap the event dated at 20.87 ± 0.46 ka cal BP, sediments that dip below the event are dated at 21.02 ± 0.47 ka cal BP (Knutz et al. (2002) seismic interpretation and ^{14}C dates; Wilson and Austin (2002) ^{14}C dates; calendar year calibration performed in this study). The primary uncertainty stems from the use of a single core and the potential complexity of the event. In conjunction with seismic data, core sample MD95-2006 brackets one lobe of the Peach 3 event; does it occur in single or multiple stages?	Knutz et al. (2002); Wilson and Austin (2002); Maslin et al. (2004); Owen (2013); this paper.
Peach 2	36.5 ka cal BP	Seismic-stratigraphic correlation based on age depth model produced by Knutz et al. (2001; 2002). Error bars are unknown, but are potentially several thousand years. This event is not sampled and the potential uncertainty is high.	Maslin et al. (2004)
Peach 1	Early to mid Pleistocene, Prior to 0.44 Ma	Interpreted, from seismic data, to contain early Pleistocene sediments and to pre-date shelf edge glaciation. This event is not sampled and age constraint is extremely loose.	Holmes et al. (1998)

Figure 1

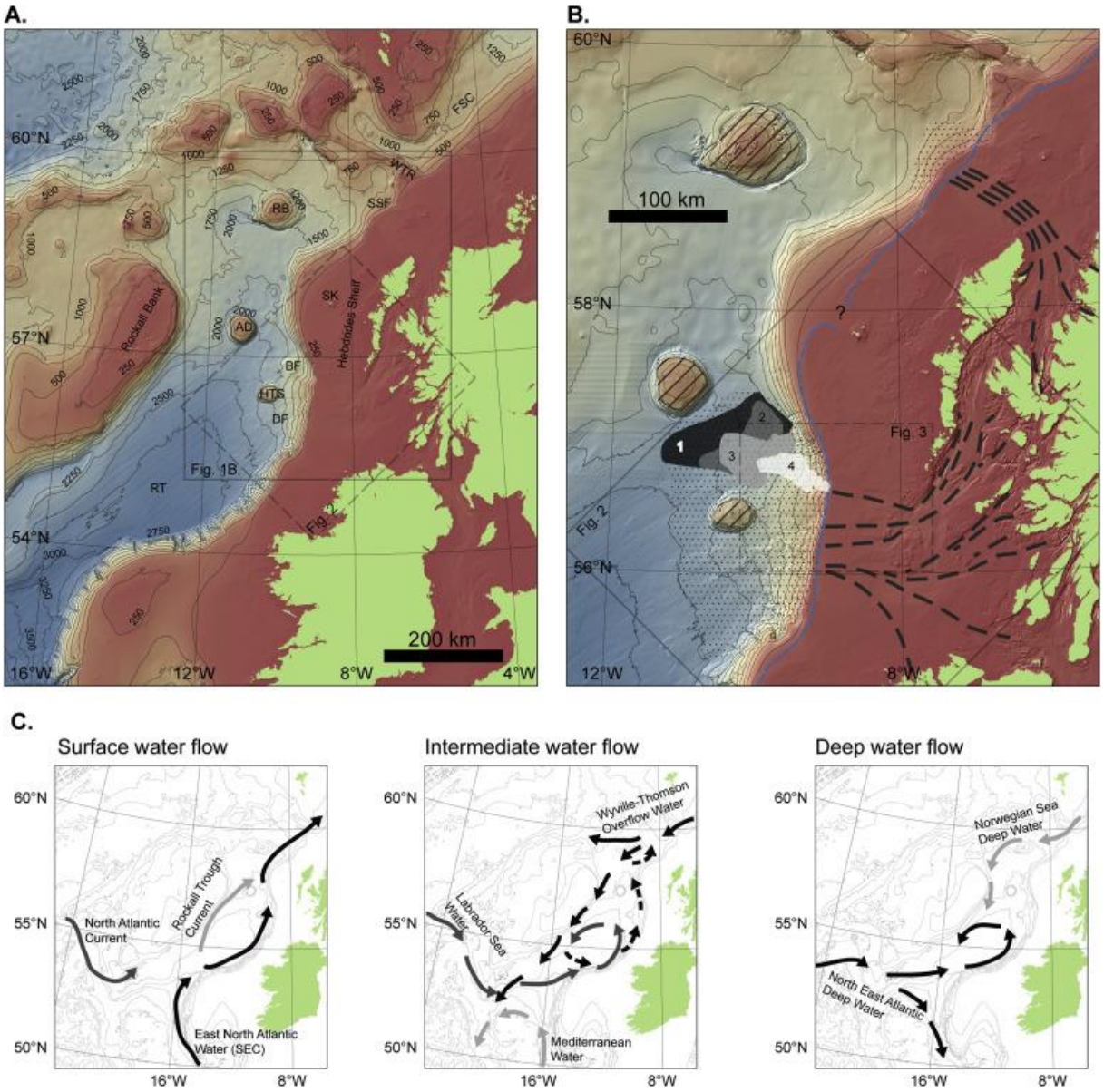
A.
B.
C.
60°N
57°N
54°N
16°W
12°W
8°W
4°W
200 km
100 km
58°N
56°N
FSC
WTR
SSF
RB
SK
AD
BF
HTS
DF
RT
Rockall Bank
Hebrides Shelf
Fig. 1B
Fig. 2
Fig. 3
Surface water flow
Intermediate water flow
Deep water flow
North Atlantic Current
Rockall Trough Current
East North Atlantic Water (SEC)
Wyville-Thomson Overflow Water
Labrador Sea Water
Mediterranean Water
Norwegian Sea Deep Water
North East Atlantic Deep Water
55°N
50°N

Figure 2

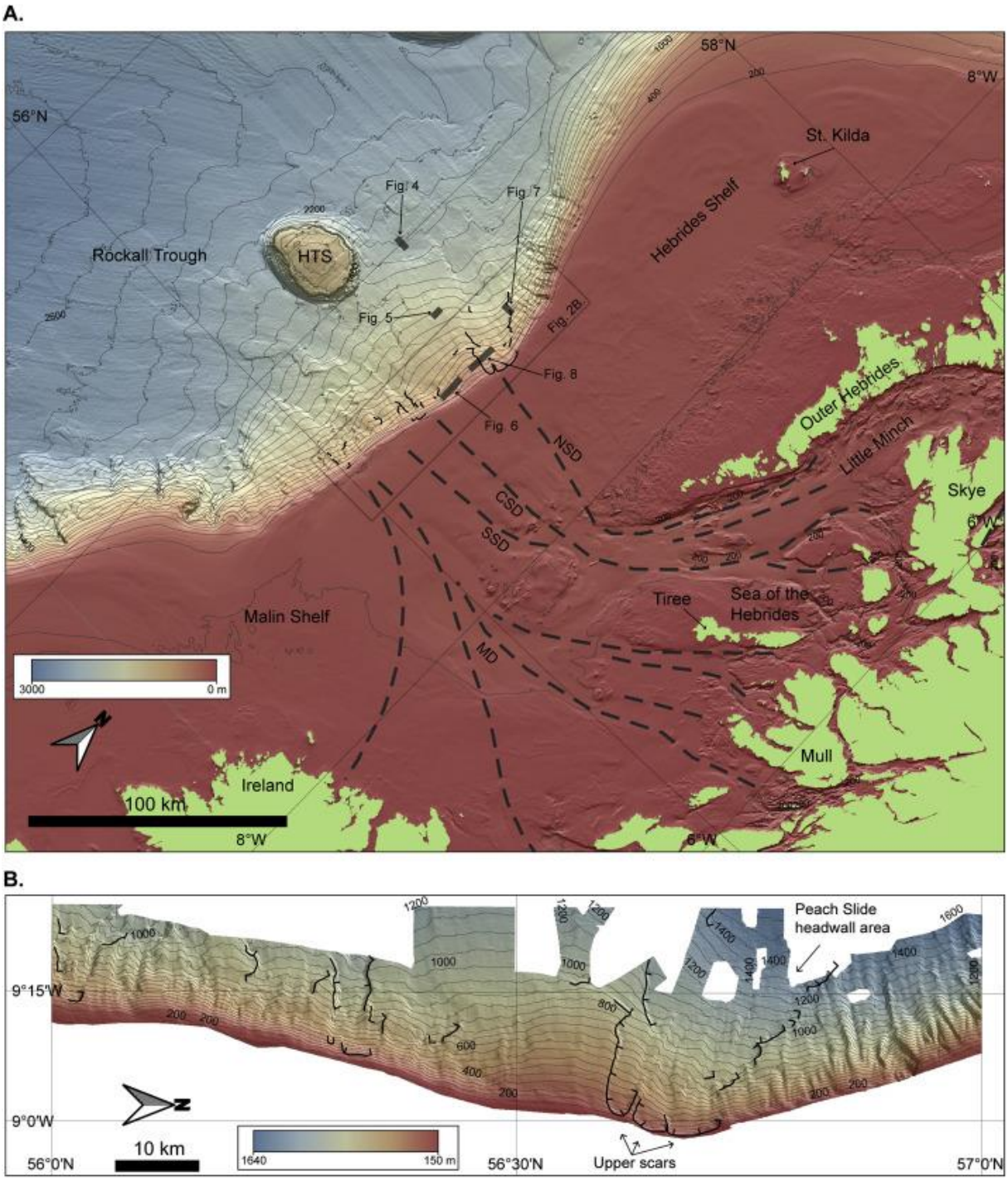
A.
58°N
8°W
56°N
St. Kilda
Fig. 4
Fig. 7
Hebrides Shelf
Rockall Trough
HTS
Fig. 5
Fig. 2B
Fig. 8
Fig. 6
Outer Hebrides
Little Minch
Skye
6°W
NSD
CSD
SSD
Tiree
Sea of the Hebrides
Malin Shelf
MD
3000
0 m
Mull
Ireland
100 km
8°W
6°W
B.
Peach Slide headwall area
9°15'W
9°0'W
56°0'N
10 km
1640
150 m
56°30'N
Upper scars
57°0'N

Figure 3

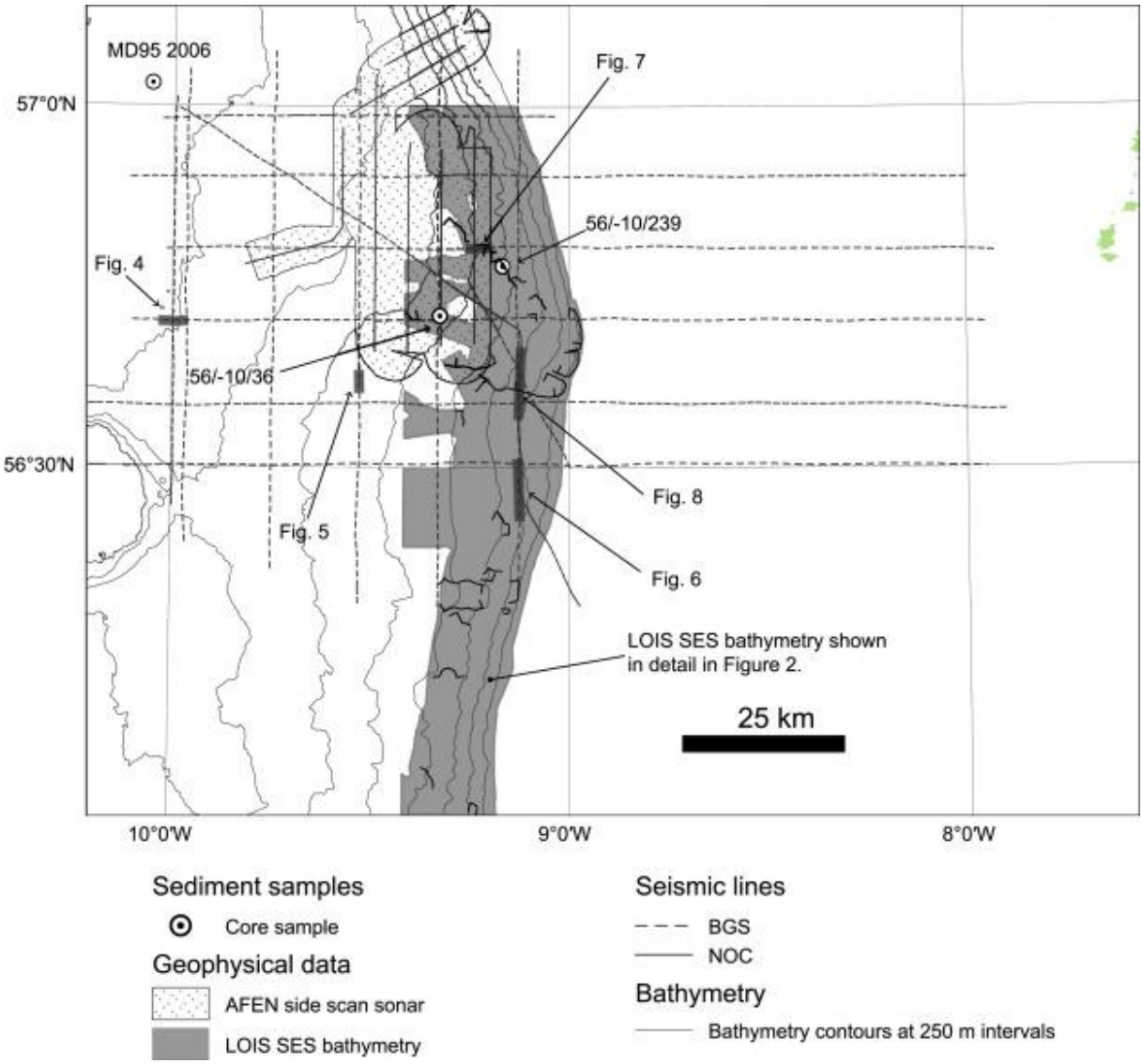
MD95 2006
57°0'N
56°30'N
Fig. 7
56/-10/239
Fig. 4
56/-10/36
Fig. 5
Fig. 8
Fig. 6
LOIS SES bathymetry shown
in detail in Figure 2.
25 km
10°0'W
9°0'W
8°0'W
Sediment samples
Core sample
Geophysical data
AFEN side scan sonar
LOIS SES bathymetry
Seismic lines
BGS
NOC
Bathymetry
Bathymetry contours at 250 m intervals

Figure 4

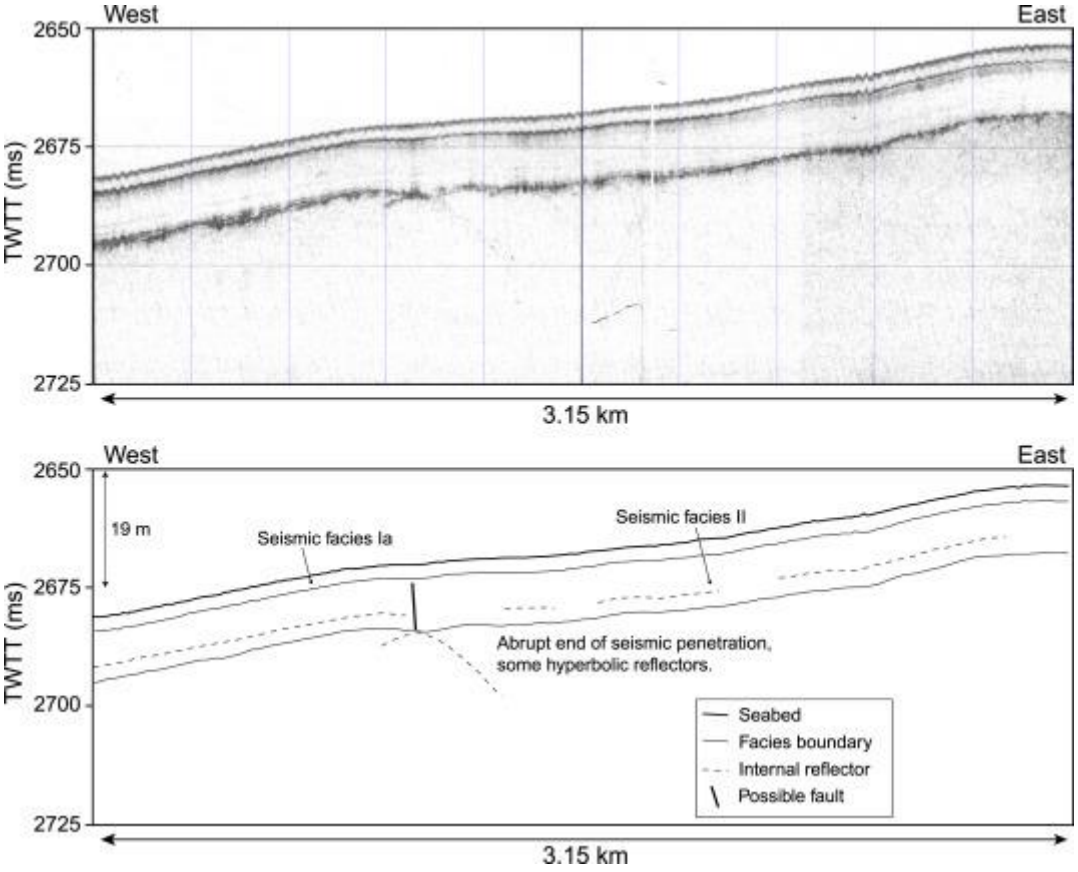
West
East
2650
2675
2700
2725
TWTT (ms)
3.15 km
West
East
19 m
Seismic facies Ia
Seismic facies II
Abrupt end of seismic penetration,
some hyperbolic reflectors.
Seabed
Facies boundary
Internal reflector
Possible fault
2650
2675
2700
2725
TWTT (ms)
3.15 km

Figure 5

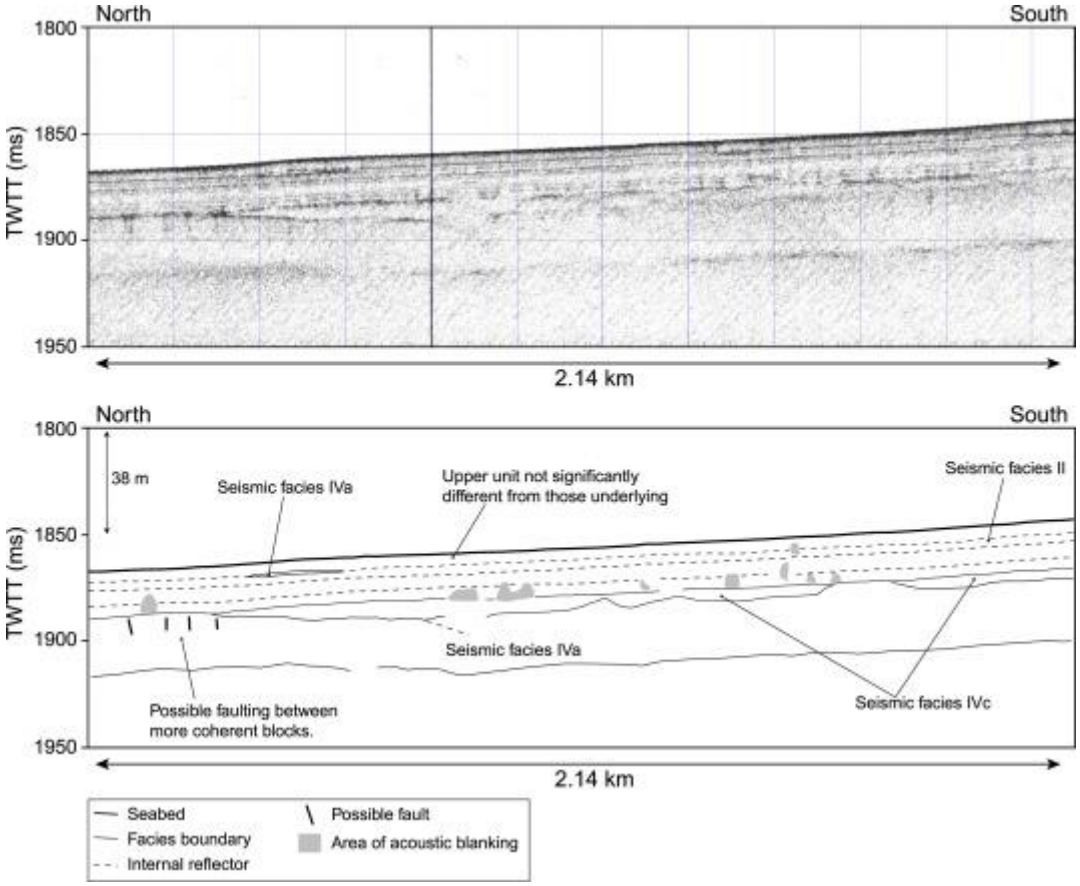
North
South
1800
1850
1900
1950
TWTT (ms)
2.14 km
North
South
38 m
Seismic facies IVa
Upper unit not significantly
different from those underlying
Seismic facies II
Seismic facies IVa
Possible faulting between
more coherent blocks.
Seismic facies IVc
2.14 km
Seabed
Facies boundary
Internal reflector
Possible fault
Area of acoustic blanking

Figure 6

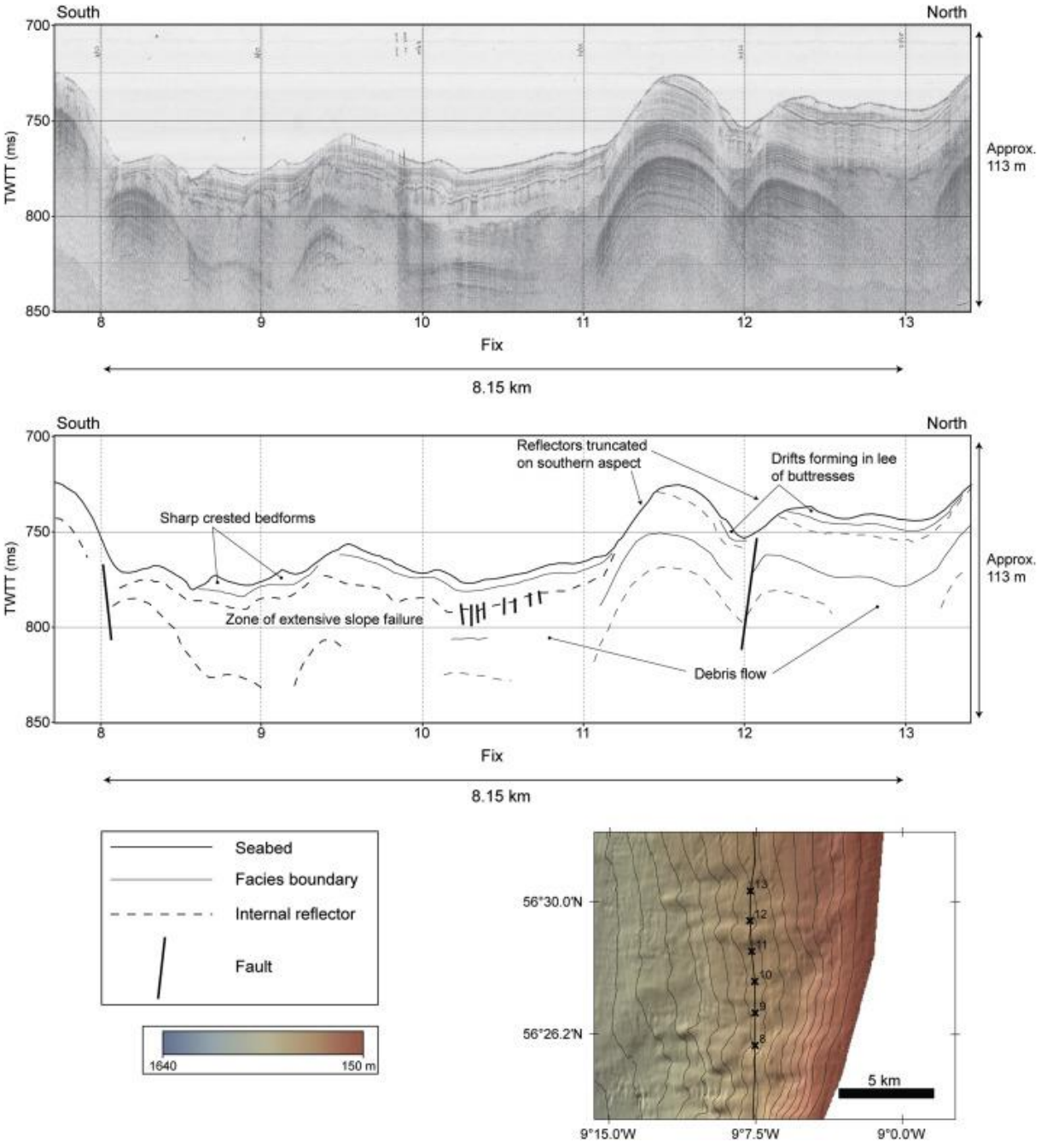
South
North
700
750
800
850
TWTT (ms)
Approx.
113 m
8
9
10
11
12
13
Fix
8.15 km
South
North
Reflectors truncated
on southern aspect
Drifts forming in lee
of buttresses
Sharp crested bedforms
Zone of extensive slope failure
Debris flow
Approx.
113 m
Fix
8.15 km
Seabed
Facies boundary
Internal reflector
Fault
1640
150 m
56°30.0'N
56°26.2'N
13
12
11
10
9
8
5 km
9°15.0'W
9°7.5'W
9°0.0'W

Figure 7

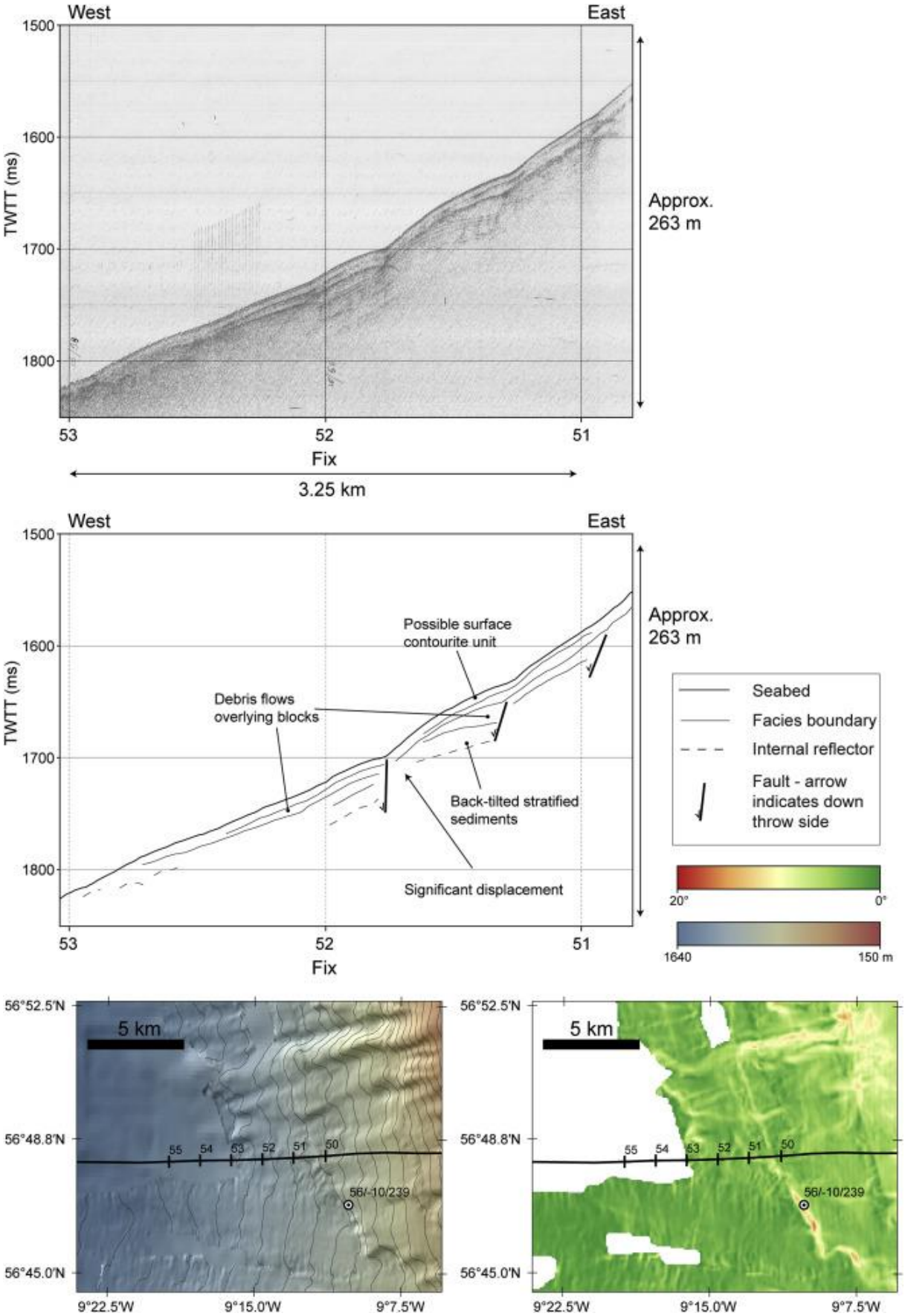
West
East
1500
1600
1700
1800
TWTT (ms)
Approx.
263 m
53
52
51
Fix
3.25 km
Possible surface
contourite unit
Debris flows
overlying blocks
Back-tilted stratified
sediments
Significant displacement
Seabed
Facies boundary
Internal reflector
Fault - arrow
indicates down
throw side
20°
0°
1640
150 m
56°52.5'N
56°48.8'N
56°45.0'N
5 km
55
54
53
52
51
50
56/-10/239
9°22.5'W
9°15.0'W
9°7.5'W

Figure 8

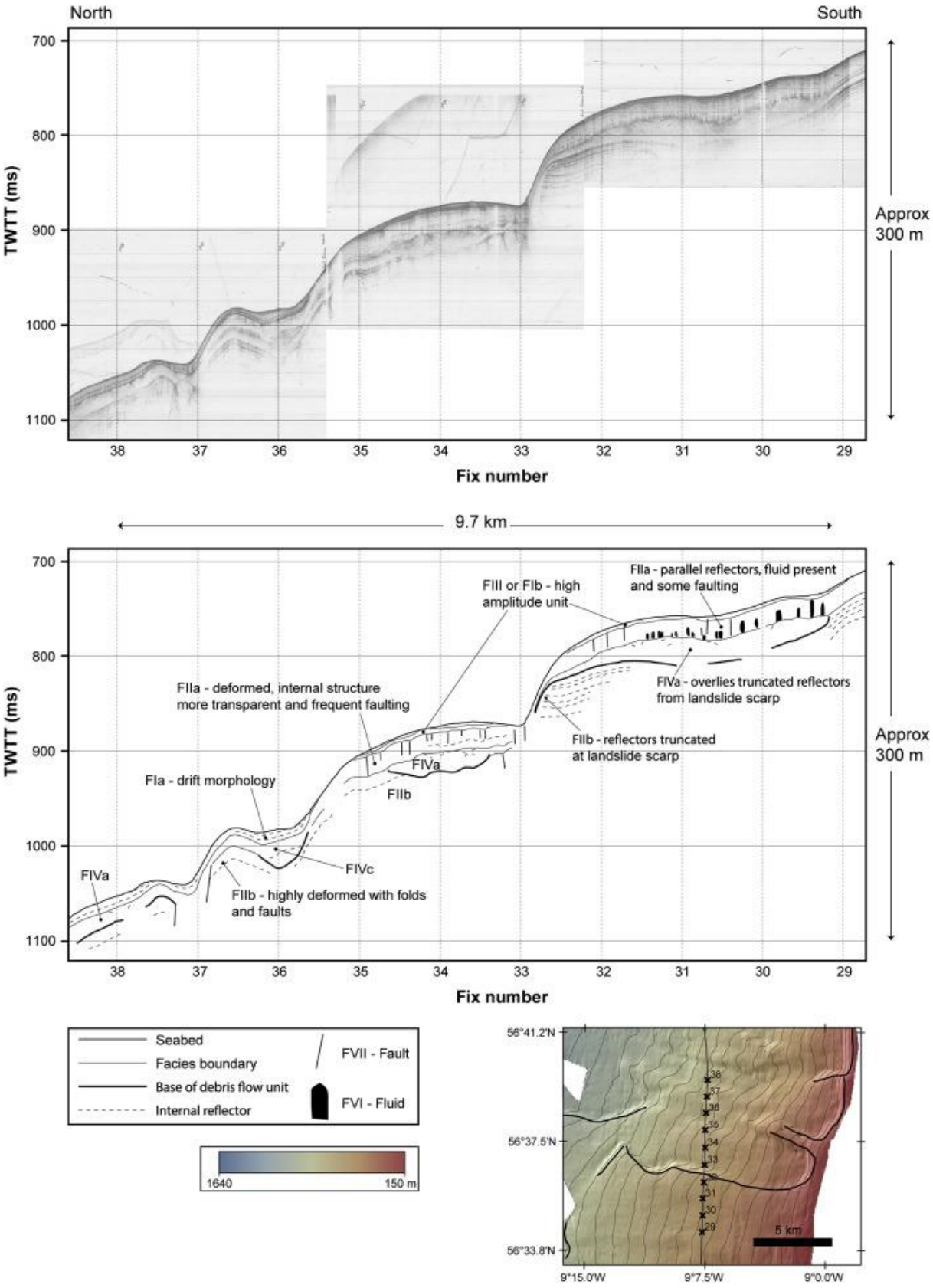
North
South
TWTT (ms)
700
800
900
1000
1100
38
37
36
35
34
33
32
31
30
29
Fix number
Approx 300 m
9.7 km
FIII or FIb - high amplitude unit
FIIa - parallel reflectors, fluid present and some faulting
FIIa - deformed, internal structure more transparent and frequent faulting
FIVa - overlies truncated reflectors from landslide scarp
FIIb - reflectors truncated at landslide scarp
FIa - drift morphology
FIVa
FIIb
FIVc
FIVa
FIIb - highly deformed with folds and faults
Seabed
Facies boundary
Base of debris flow unit
Internal reflector
FVII - Fault
FVI - Fluid
1640
150 m
56°41.2'N
56°37.5'N
56°33.8'N
9°15.0'W
9°7.5'W
9°0.0'W
5 km

Figure 9

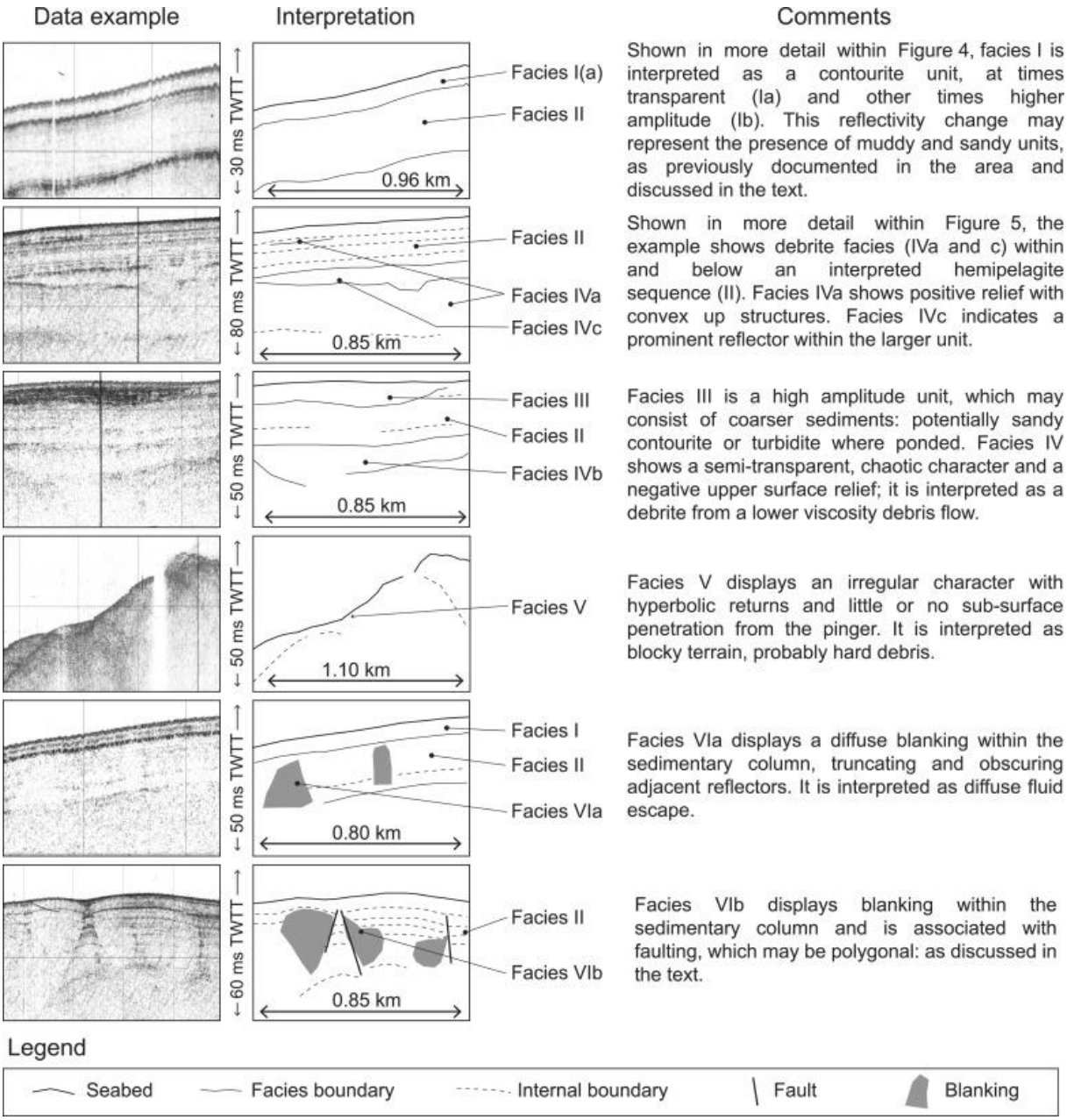
Data example
Interpretation
Comments
30 ms TWTT
0.96 km
Facies I(a)
Facies II
Shown in more detail within Figure 4, facies I is interpreted as a contourite unit, at times transparent (Ia) and other times higher amplitude (Ib). This reflectivity change may represent the presence of muddy and sandy units, as previously documented in the area and discussed in the text.
80 ms TWTT
0.85 km
Facies II
Facies IVa
Facies IVc
Shown in more detail within Figure 5, the example shows debrite facies (IVa and c) within and below an interpreted hemipelagite sequence (II). Facies IVa shows positive relief with convex up structures. Facies IVc indicates a prominent reflector within the larger unit.
50 ms TWTT
0.85 km
Facies III
Facies II
Facies IVb
Facies III is a high amplitude unit, which may consist of coarser sediments: potentially sandy contourite or turbidite where ponded. Facies IV shows a semi-transparent, chaotic character and a negative upper surface relief; it is interpreted as a debrite from a lower viscosity debris flow.
50 ms TWTT
1.10 km
Facies V
Facies V displays an irregular character with hyperbolic returns and little or no sub-surface penetration from the pinger. It is interpreted as blocky terrain, probably hard debris.
50 ms TWTT
0.80 km
Facies I
Facies II
Facies VIa
Facies VIa displays a diffuse blanking within the sedimentary column, truncating and obscuring adjacent reflectors. It is interpreted as diffuse fluid escape.
60 ms TWTT
0.85 km
Facies II
Facies VIb
Facies VIb displays blanking within the sedimentary column and is associated with faulting, which may be polygonal: as discussed in the text.
Legend
Seabed
Facies boundary
Internal boundary
Fault
Blanking

Figure 10

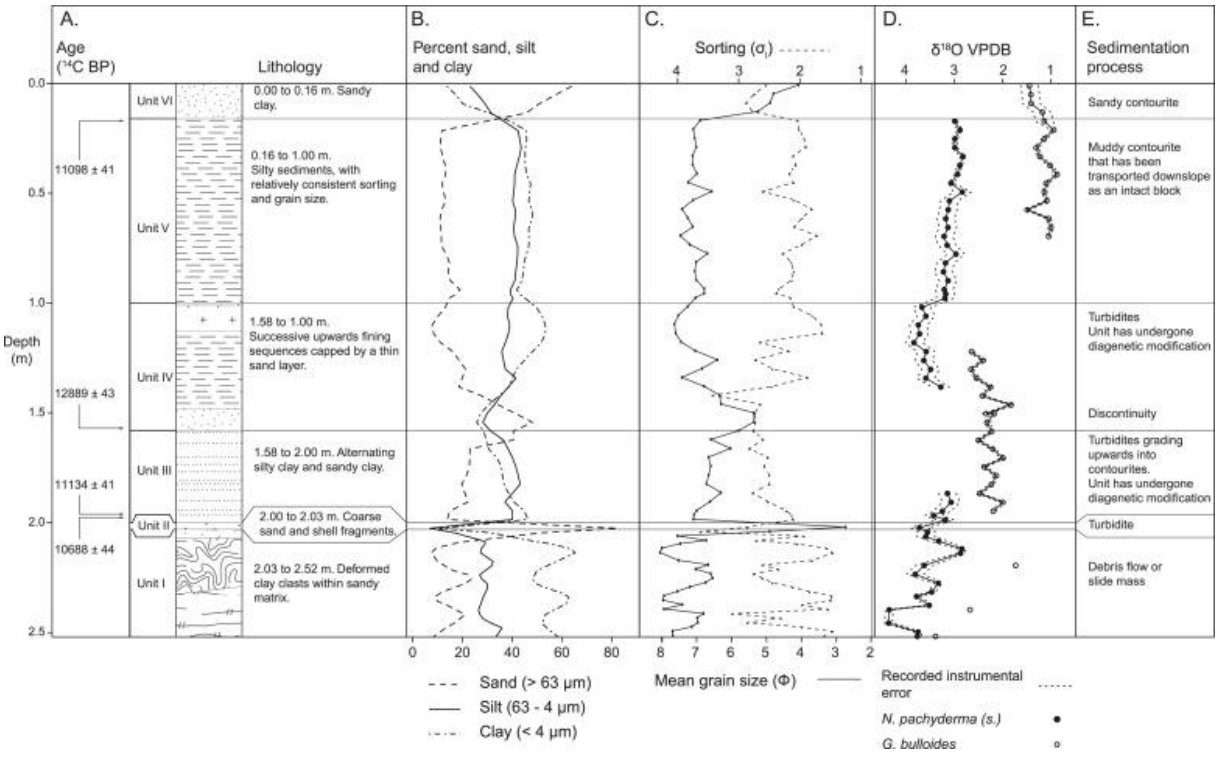
A.
Age
(14C BP)
Lithology
B.
Percent sand, silt
and clay
C.
Sorting (σi)
D.
δ18O VPDB
E.
Sedimentation
process
Depth
(m)
0.0
0.5
1.0
1.5
2.0
2.5
11098 ± 41
12889 ± 43
11134 ± 41
10688 ± 44
Unit VI
Unit V
Unit IV
Unit III
Unit II
Unit I
0.00 to 0.16 m. Sandy clay.
0.16 to 1.00 m.
Silty sediments, with relatively consistent sorting and grain size.
1.58 to 1.00 m.
Successive upwards fining sequences capped by a thin sand layer.
1.58 to 2.00 m. Alternating silty clay and sandy clay.
2.00 to 2.03 m. Coarse sand and shell fragments.
2.03 to 2.52 m. Deformed clay clasts within sandy matrix.
Sandy contourite
Muddy contourite that has been transported downslope as an intact block
Turbidites
Unit has undergone diagenetic modification
Discontinuity
Turbidites grading upwards into contourites.
Unit has undergone diagenetic modification
Turbidite
Debris flow or slide mass
0 20 40 60 80
Sand (> 63 μm)
Silt (63 - 4 μm)
Clay (< 4 μm)
8 7 6 5 4 3 2
Mean grain size (Φ)
Recorded instrumental error
N. pachyderma (s.)
G. bulloides

Figure 11

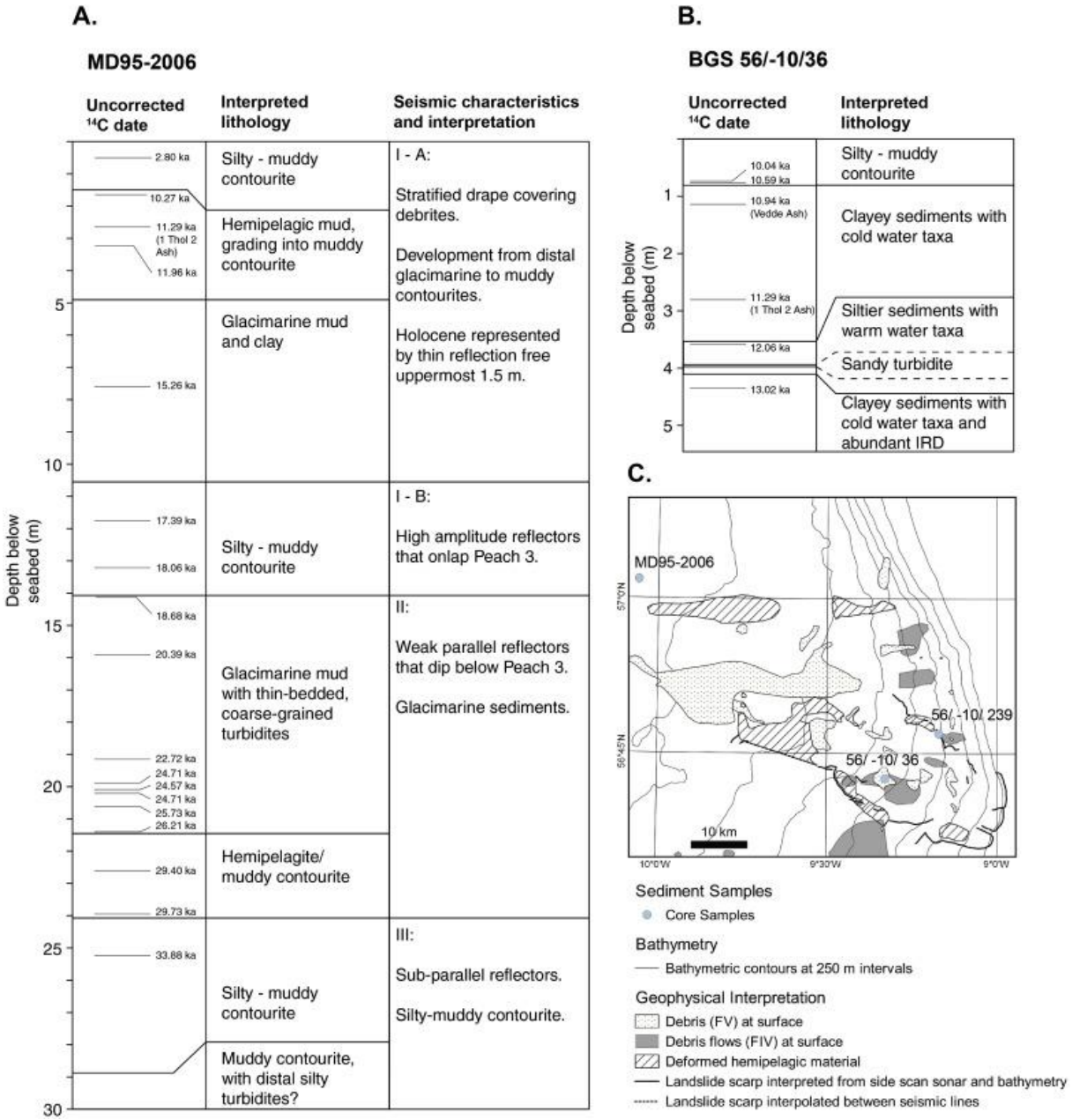
A.
MD95-2006
Uncorrected ¹⁴C date
Interpreted lithology
Seismic characteristics and interpretation
Depth below seabed (m)
2.80 ka
10.27 ka
11.29 ka (1 Thol 2 Ash)
11.96 ka
15.26 ka
17.39 ka
18.06 ka
18.68 ka
20.39 ka
22.72 ka
24.71 ka
24.57 ka
24.71 ka
25.73 ka
26.21 ka
29.40 ka
29.73 ka
33.88 ka
Silty - muddy contourite
Hemipelagic mud, grading into muddy contourite
Glacimarine mud and clay
Silty - muddy contourite
Glacimarine mud with thin-bedded, coarse-grained turbidites
Hemipelagite/ muddy contourite
Silty - muddy contourite
Muddy contourite, with distal silty turbidites?
I - A:
Stratified drape covering debrites.
Development from distal glacimarine to muddy contourites.
Holocene represented by thin reflection free uppermost 1.5 m.
I - B:
High amplitude reflectors that onlap Peach 3.
II:
Weak parallel reflectors that dip below Peach 3.
Glacimarine sediments.
III:
Sub-parallel reflectors.
Silty-muddy contourite.
B.
BGS 56/-10/36
Uncorrected ¹⁴C date
Interpreted lithology
Depth below seabed (m)
10.04 ka
10.59 ka
10.94 ka (Vedde Ash)
11.29 ka (1 Thol 2 Ash)
12.06 ka
13.02 ka
Silty - muddy contourite
Clayey sediments with cold water taxa
Siltier sediments with warm water taxa
Sandy turbidite
Clayey sediments with cold water taxa and abundant IRD
C.
MD95-2006
56/ -10/ 239
56/ -10/ 36
10 km
10°0'W
9°30'W
9°0'W
57°0'N
56°45'N
Sediment Samples
Core Samples
Bathymetry
Bathymetric contours at 250 m intervals
Geophysical Interpretation
Debris (FV) at surface
Debris flows (FIV) at surface
Deformed hemipelagic material
Landslide scarp interpreted from side scan sonar and bathymetry
Landslide scarp interpolated between seismic lines

Figure 12

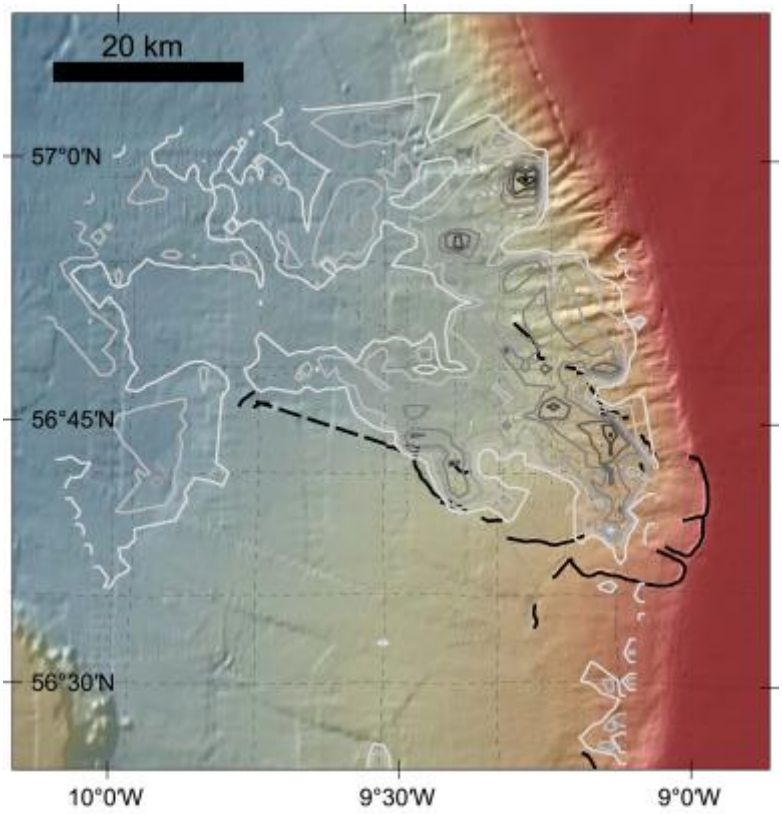

Geophysical data

Seismic survey lines

Surface interpretation

Landslide scarp from side scan sonar and bathymetry

Landslide scarp interpolated between seismic lines

Thickness of contourite unit (m)

2 6

3 7

4 8

5 9

Water depth (m)

2500 150 m

Figure 13

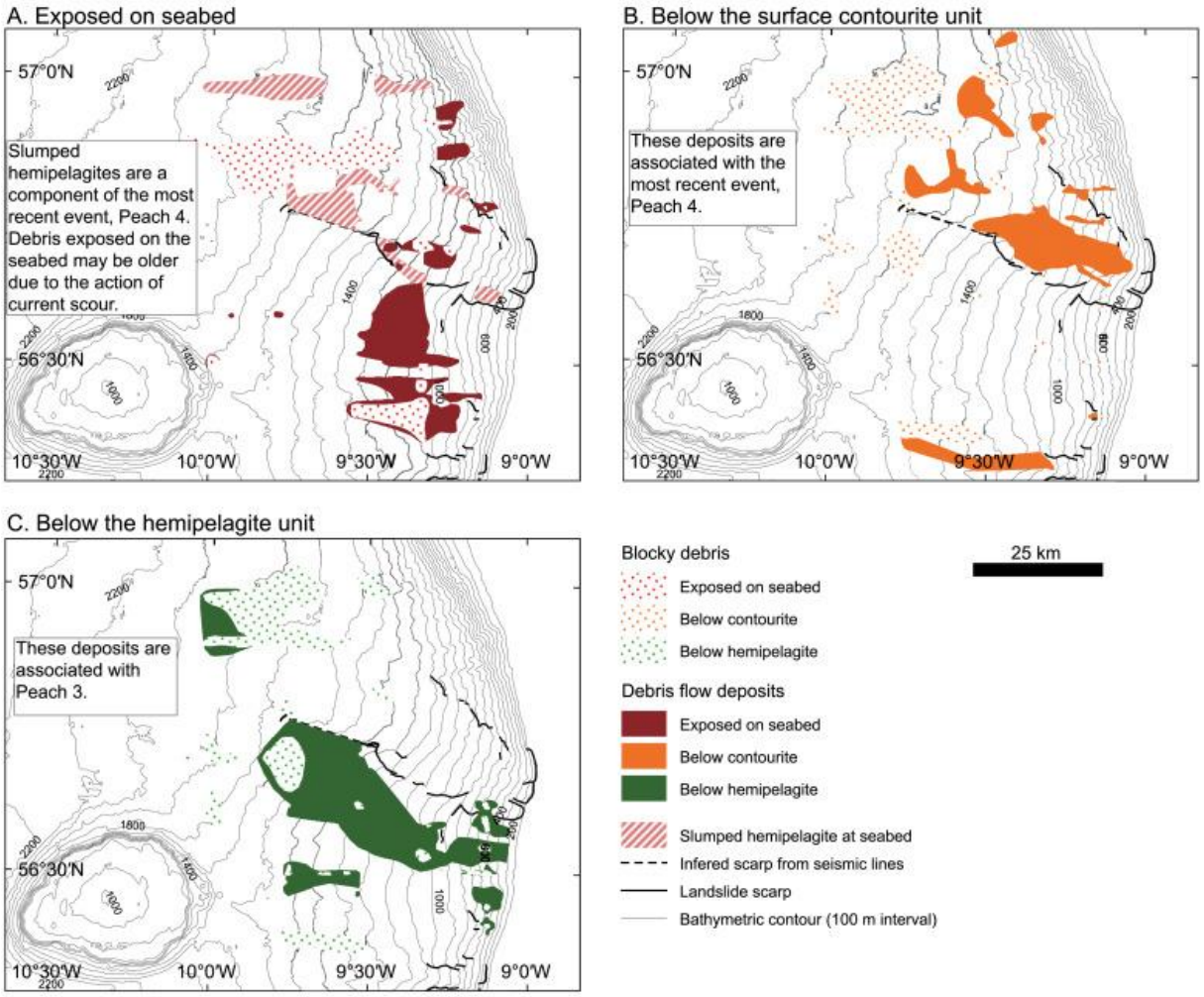
A. Exposed on seabed
Slumped hemipelagites are a component of the most recent event, Peach 4. Debris exposed on the seabed may be older due to the action of current scour.
B. Below the surface contourite unit
These deposits are associated with the most recent event, Peach 4.
C. Below the hemipelagite unit
These deposits are associated with Peach 3.
57°0'N
56°30'N
10°30'W
10°0'W
9°30'W
9°0'W
Blocky debris
Exposed on seabed
Below contourite
Below hemipelagite
Debris flow deposits
Exposed on seabed
Below contourite
Below hemipelagite
Slumped hemipelagite at seabed
Infered scarp from seismic lines
Landslide scarp
Bathymetric contour (100 m interval)
25 km

Figure 14

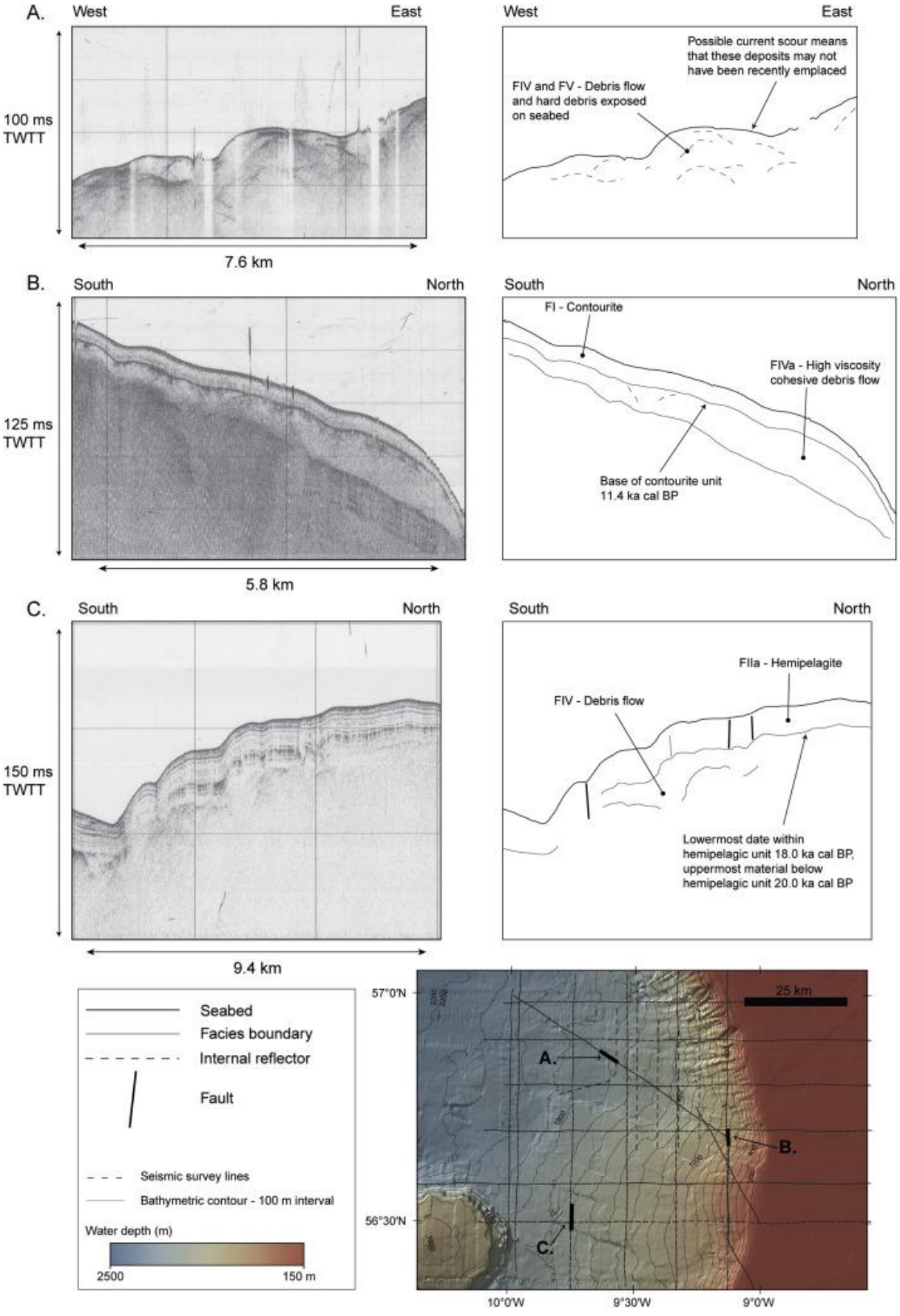
A.
West
East
100 ms
TWTT
7.6 km
West
East
Possible current scour means that these deposits may not have been recently emplaced
FIV and FV - Debris flow and hard debris exposed on seabed
B.
South
North
125 ms
TWTT
5.8 km
South
North
FI - Contourite
FIVa - High viscosity cohesive debris flow
Base of contourite unit 11.4 ka cal BP
C.
South
North
150 ms
TWTT
9.4 km
South
North
FIIa - Hemipelagite
FIV - Debris flow
Lowermost date within hemipelagic unit 18.0 ka cal BP, uppermost material below hemipelagic unit 20.0 ka cal BP
Seabed
Facies boundary
Internal reflector
Fault
Seismic survey lines
Bathymetric contour - 100 m interval
Water depth (m)
2500
150 m
57°0'N
56°30'N
25 km
A.
B.
C.
10°0'W
9°30'W
9°0'W

Figure 15

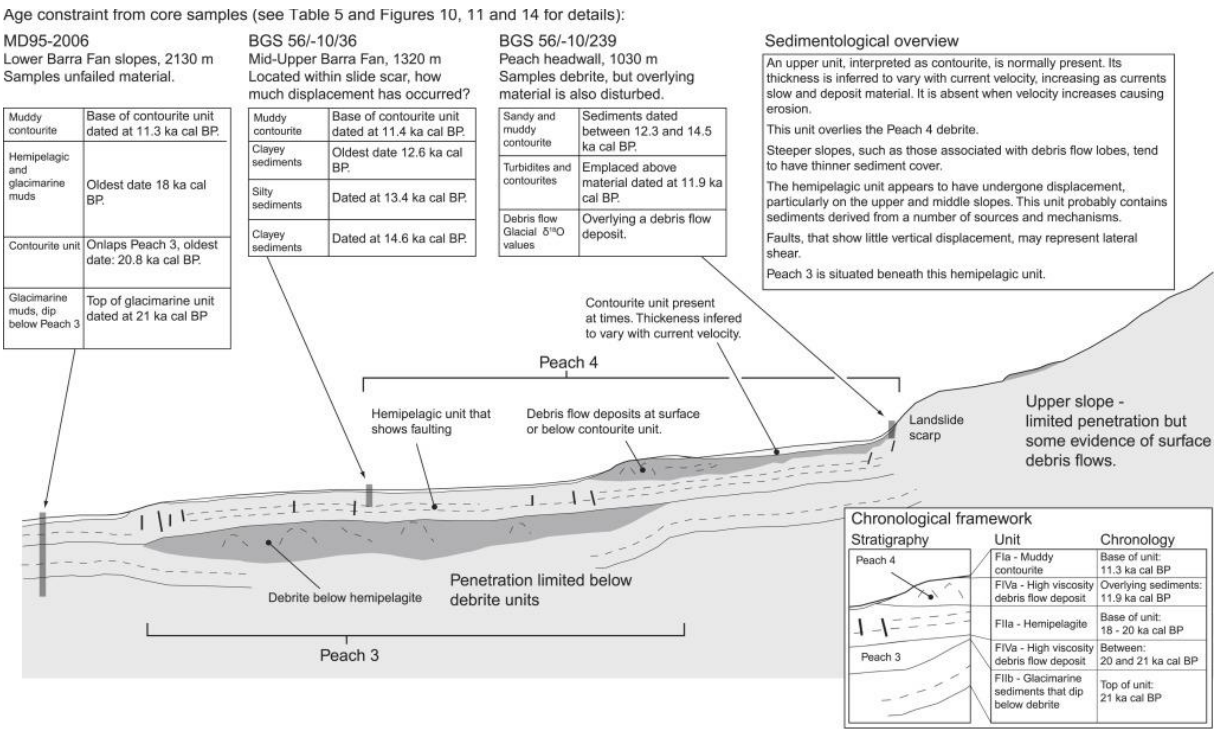
Age constraint from core samples (see Table 5 and Figures 10, 11 and 14 for details):
MD95-2006
Lower Barra Fan slopes, 2130 m
Samples unfailed material.
Muddy contourite
Base of contourite unit dated at 11.3 ka cal BP.
Hemipelagic and glacimarine muds
Oldest date 18 ka cal BP.
Contourite unit
Onlaps Peach 3, oldest date: 20.8 ka cal BP.
Glacimarine muds, dip below Peach 3
Top of glacimarine unit dated at 21 ka cal BP
BGS 56/-10/36
Mid-Upper Barra Fan, 1320 m
Located within slide scar, how much displacement has occurred?
Muddy contourite
Base of contourite unit dated at 11.4 ka cal BP.
Clayey sediments
Oldest date 12.6 ka cal BP.
Silty sediments
Dated at 13.4 ka cal BP.
Clayey sediments
Dated at 14.6 ka cal BP.
BGS 56/-10/239
Peach headwall, 1030 m
Samples debrite, but overlying material is also disturbed.
Sandy and muddy contourite
Sediments dated between 12.3 and 14.5 ka cal BP.
Turbidites and contourites
Emplaced above material dated at 11.9 ka cal BP.
Debris flow Glacial δ18O values
Overlying a debris flow deposit.
Sedimentological overview
An upper unit, interpreted as contourite, is normally present. Its thickness is inferred to vary with current velocity, increasing as currents slow and deposit material. It is absent when velocity increases causing erosion.
This unit overlies the Peach 4 debrite.
Steeper slopes, such as those associated with debris flow lobes, tend to have thinner sediment cover.
The hemipelagic unit appears to have undergone displacement, particularly on the upper and middle slopes. This unit probably contains sediments derived from a number of sources and mechanisms.
Faults, that show little vertical displacement, may represent lateral shear.
Peach 3 is situated beneath this hemipelagic unit.
Contourite unit present at times. Thickeness infered to vary with current velocity.
Peach 4
Hemipelagic unit that shows faulting
Debris flow deposits at surface or below contourite unit.
Landslide scarp
Upper slope - limited penetration but some evidence of surface debris flows.
Debrite below hemipelagite
Penetration limited below debrite units
Peach 3
Chronological framework
Stratigraphy
Unit
Chronology
Peach 4
FIa - Muddy contourite
Base of unit: 11.3 ka cal BP
FIVa - High viscosity debris flow deposit
Overlying sediments: 11.9 ka cal BP
FIIa - Hemipelagite
Base of unit: 18 - 20 ka cal BP
Peach 3
FIVa - High viscosity debris flow deposit
Between: 20 and 21 ka cal BP
FIIb - Glacimarine sediments that dip below debrite
Top of unit: 21 ka cal BP

Figure 16

Time Period		British-Irish Ice Sheet	Slope parallel currents	Sedimentation regime	Pre-conditioning factors and trigger mechanisms	Mass movement event
Intra-Pliocene unconformity	4 ± 0.5 Ma	Not present	Bottom current activity interpreted from seismo- stratigraphic record.	Initiation of slope front fan development on NW European margin via uplift and increased runoff.	Before the focus of this study, but sediment accumulation and fan development would lead to the potential for slope failures.	None known.
Early Pleistocene	2.6 Ma	Evidence that a marine terminating ice-sheet is occassionally present.	Circulation pattern likely to become more similar to that seen in later Pleistocene stadial and inter-stadial, with increasing differences between warm and cold periods as glaciations intensify.	Deposition of the Lower MacLeod sequence of shallow marine sands. Likely to be some glacial influence.	Build up of fan sediments, with the potential for some lower permeability layers. Intensification of northern hemispheric glaciations allow for potential eustatic sea-level changes and related effects on sedimentation and gas hydrates.	Peach 1 potentially occurs during this interval, the actual timing is highly uncertain.
Intra-Pleistocene unconformity	0.44 Ma	Intensified glaciations leading to the beginning of the period of intermittent shelf edge ice-sheets.	Circulation pattern likely to be similar to that seen in most recent Pleistocene stadial and inter-stadial periods.	Deposition of the Upper MacLeod sequence of glacial muds. Contourite and hemipelagite deposition is likely to occur during interglacial and deglacial periods.	Development of lower porosity units associated with inter-stadial periods, and rapid sedimentary loading associated with glacigenic sedimentation during stadials (and ice-sheet collapse in particular). Potential for isostatic and eustatic effects influencing gas hydrates and seismicity as well as glacitectonic faulting. Possible undercutting by currents during inter-stadials. Such factors are amplified by increased intensity of glaciations and the advent of shelf-edge ice.	None known, though glacigenic debris flows are likely. Other events may be obscured by later debrites.
Establishment of the latest phase of the BIIS	46 ka	BIIS undergoes expansion, with a significant increase in IRD at 41 ka cal BP.	Increasingly sluggish as glaciation intensifies, though perhaps increased velocity associated with D-O events.	Sedimentation dominated by glacigenic processes. The rate is anticipated to increase as the ice-front nears the shelf edge.		Peach 2 occurs circa 36.5 ka cal BP (considerable potential for error).
BIIS LGM	27 - 24 ka	Ice present at the shelf edge, with streaming from western Scotland, the North Channel and Malin.		Glacimarine sedimentation, rapid sedimentation rates.		
BIIS retreat from shelf edge to mainland.	24 - 16.5 ka	Rapid retreat of HIS, Tiree exposed at 20.6 ka cal BP. Onshore ice-sheet by 15.5 ka cal BP.	Reinvigouration of bottom current flow, sluggish again during Heinrich 1.	Extremely rapid deglacial sedimentation associated with initial retreat. Followed by contouritic and hemipelagic sedimentaion.	Fluctuating sedimentation regime constructs a high porosity - low permeability sequence. Rapid deposition of final periglacial sediments generating excess pore pressure. Earlier slide phases create locally steep slopes and water column turbulence that facilitates silt deposition. Ongoing isostatic adjustments allow possible roles for seismicity and glacitectonic faulting.	Peach 3 occurs circa 21.0 ka cal BP (see Table 5 and text for discussion). Some evidence of debris flows within deglacial sequence.
Bølling Allerød	14.6 - 13.5 ka	A shrinking terrestrial ice-sheet.	Vigourous flow.	Contouritic and hemipelagic sedimentaion.		
Younger Dryas	13.5 - 10.9 ka	Resumption of ice-berg calving in western Scotland.	Sluggish flow.	Glacigenic sedimentation, rates >2.0 m ka^{-1}.		Peach 4 occurs between 12 and 11 ka cal BP (see Table 5 and text for discussion).
Holocene	10.9 ka to modern	Ice retreats.	Vigourous flow.	Contouritic and hemipelagic sedimentaion.	Deposition of high porosity sediments, warmer water masses may influence gas hydrates. Role for isostatic adjustment in the early part of the period.	Possible minor sediment failures as slide scar stabilises.